January 10, 1974

A Thesis

entitled

The Surface Brightness of Reflection Nebulae

by

William F. Rush

NGR-36-010-016
Univ. of Toledo

as partial fulfillment of the requirements of
the Doctor of Philosophy Degree in
Physics and Astronomy

Adolf N. Witt
Advisor

Dean of the Graduate School

The University of Toledo
December, 1972

ABSTRACT

Hubble's equation relating the maximum apparent angular extent of a reflection nebula to the apparent magnitude of the illuminating star has been reconsidered under a set of less restrictive assumptions. A computational technique is developed which permits the use of fits to observed m, log a values to determine the albedo of the particles composing reflection nebulae, providing only that one assumes a particular phase function. Despite the fact that all orders of scattering, anisotropic phase functions, and illumination by the general stellar field are considered, the albedo which is determined for reflection nebulae by this method appears larger than that for interstellar particles in general. The possibility that the higher surface brightness might be due to a continuous fluorescence mechanism is considered both theoretically and observationally.

From the observations, the ratio of fluorescent to reflected contribution to nebular surface brightness is found to be zero with an rms deviation corresponding to .1. The calculations indicate that this ratio must be at least .3 if the albedo of nebular particles is to be the same as the albedo of general interstellar particles. These results imply that:

1. The fluorescent mechanism considered here and elsewhere to explain the high surface brightness of reflection nebulae is not, in fact, operative to the extent required to explain the observed surface brightness of reflection nebulae.

2. The albedo of particles in reflection nebulae is probably higher than the value typical of general interstellar particles.

ACKNOWLEDGEMENTS

It is a great pleasure to thank Dr. Adolf Witt for introducing me to this problem and for his continued guidance and criticism. Helpful discussions with Dr. Conard Dahn and Dr. C. R. O'Dell are gratefully acknowledged. The funds provided by NASA Grant No. NGR 36-010-016 for the purchase of the interference filters are very much appreciated. I am very grateful for the travel funds provided by AURA and the University of Toledo. The observing time and the enthusiastic and helpful support given to me by the staff of the Kitt Peak National Observatory are deeply appreciated. Finally, I wish to thank my wife, Anita, for her continued patience and support during the many difficulties encountered during this investigation.

TABLE OF CONTENTS

TABLE OF FIGURES

TABLE OF FIGURES

(cont.)

TABLE OF TABLES

I. INTRODUCTION

1. Reflection Nebulae and Interstellar Particles

Interstellar grains are not distributed homogeneously in space, but often tend to occur in clouds whose dimensions are on the order of 10 parsecs. A chance proximity between such a cloud and a star would produce a reflection nebula, i.e., a nebula whose emerging radiation is reflected starlight. An analysis by Ambartsumian and Gordeladse (1938) indicates that the observed number of reflection nebulae is consistent with chance associations between the interstellar clouds and stars. If the illuminating star has a sufficient ultraviolet photon flux, the hydrogen which always accompanies the interstellar dust, will be excited, resulting in an emission nebula. A star which is too faint will not produce sufficient light to make the nebula observable. Hence, most reflection nebulae are illuminated by main sequence stars of spectral type A or B or by late type giants. There are many cases, however, in which an actual physical relationship between the star and the reflection nebula must be suspected. Racine (1968) finds that reflection nebulae are frequently clustered together in "R associations" which are found along spiral arms. In short, although there is no evidence to indicate that reflection nebulae are not typical of the interstellar medium, it is possible that their grains could be different. However, this is a conclusion to which one would come only after other possibilities have been thoroughly investigated.

A major impetus for the work which is described in this paper is to gain information concerning the nature of the particles which make up reflection nebulae and thus to try to learn more about interstellar particles in general. Of course, some of the most interesting and fundamental questions which one can ask about interstellar particles concern

their chemical composition and size distribution. However, the approach which has been used here is to attempt to deduce information about the albedo and scattering properties of reflection nebula particles. This information could then be used to discriminate among various models for the particles.

Reflection nebulae provide an opportunity to investigate light which has been scattered by interstellar grains which is almost unique. Only in the cases of diffuse galactic light and dark nebulae can one otherwise observe scattered light. Extinction studies, in which one observes the spectrum of a star lying behind some interstellar particles, allow one to study only the light which has been transmitted through the material, while scattered light observations allow investigation of the light which has interacted with the grains.

2. Observations of Interstellar Particles

Interstellar extinction, polarization, and scattered light are the main observational bases on which our ideas concerning the interstellar particles are founded. These observations will be discussed below.

a) Extinction

Extinction is a general term which is applied to the dimming of starlight which travels through the interstellar medium. It should be noted that starlight could be dimmed in either of two ways: first, it might experience a true absorption in which a photon of one frequency is absorbed and reemitted at another frequency (and a different direction), and second, it may be reemitted at the same frequency but in a different direction. The first process is called true absorption and

the second is called scattering. Since it is not known to what extent each process is responsible for the observed dimming of starlight, the term extinction is used to describe the process in order to avoid semantic confusion.

At this point it is convenient to define some quantities which will be used later. Let σ be the geometric cross section of a particle and let C be the total cross section for some process (absorption or scattering). Then we will define the efficiency, Q, for that process by

$$Q = \frac{C}{\sigma} \quad . \tag{1}$$

From our discussion of extinction and the definition of equation 1), it follows that

$$Q_{ext} = Q_{sca} + Q_{abs} \quad , \tag{2}$$

the subscripts having the obvious meanings. It should be noted here that the tacit assumption is being made that light is either absorbed or scattered, but not emitted. Extinction is wavelength dependent and this dependence results in a reddening of starlight. It is found that the extinction follows roughly a $1/\lambda$ law in the visible region of the spectrum. It should be noted that these observations are made with broad band filters (500 to 1000 Å) and consequently are not capable of revealing any detail in the extinction curve. In the ultraviolet, the extinction curve begins to show some structure, as shown in Figure I.

More recent studies by York (1971) and Walker, et al. (1969) have shown that the interstellar extinction curve has considerable amounts of fine structure when examined at higher resolution. In

general, one finds rather broad features (20 to 200 Å) separated by relatively smooth stretches in the curve. Walker, et al., find many changes of slope in the curve, a few of which are associated with the "diffuse interstellar features". There are approximately 25 of these diffuse features in the visible region. The strongest of these features is at λ 4430 Å. For reflection nebulae, the detection of an absorption feature at λ 4430 Å by A'Hearn (1971) is important in that it provides an indication that interstellar grains and reflection nebulae particles might be similar.

b) Polarization

The second group of observations which bear on the nature of interstellar particles is polarization measurements. These measurements will not be considered in very much detail here, since they do not have a strong impact on the particular problem which is being considered. For our purposes it will be sufficient to remark that partial linear polarization is observed in many stars and the directions of polarization are correlated over large areas of the sky. Polarization is often correlated with extinction, and as might be expected, has never been observed without accompanying extinction.

One implication of polarization observations is that the interstellar grains must have some intrinsic anisotropy in shape or optical properties. There must also exist some preferred spatial direction in the galaxy, defined by an alignment mechanism (such as, perhaps, a magnetic field).

c) Scattered Light Observations

In addition to extinction and polarization, the third set of observations which are important to our understanding of the interstellar

grains concerns scattered light. For both extinction and polarization measurements, the star, the grains and the observer all share a common line of sight. Since both scattering and absorption could produce the observed features, it is difficult to study the details of interaction between light and interstellar grains. If we can by some method restrict ourselves to only that light which we know has been scattered, one uncertainty has been eliminated.

In the study of scattered light, two parameters are of fundamental importance: the albedo and the phase function. The albedo is a measure of the reflectivity of the particle and is defined as

$$\gamma = \frac{Q_{sca}}{Q_{abs} + Q_{sca}} \quad . \tag{3}$$

Note that γ is unity for a particle which does not absorb and it approaches zero for very large absorption efficiencies. The phase function is a "weighting function" which describes what fraction of the scattered intensity is scattered into each final direction, normalized so that

$$\int P(\cos\theta) \frac{d\omega}{4\pi} = \gamma \quad , \tag{4}$$

where θ is the scattering angle and $P(\cos\theta)$ is the phase function. (See Chandrasekhar,(1950), pg. 6). In practice, the phase function itself is rarely used because it tends to be rather unwieldy. Phase functions for particles about the size of the wavelength of light often have six or more oscillations in their curve of $P(\theta)$ as a function of θ, as shown by Plass (1966). Instead, most authors follow Henyey and Greenstein (1941) and use the "asymmetry parameter" g, defined by

$$g = \frac{1}{\gamma} \int P(\cos\theta) \cos\theta \frac{d\omega}{4\pi} \quad . \tag{5}$$

So defined, g is the weighted mean of cos θ with $P(\cos \theta)$ as the weighting function. It is zero for an isotropic phase function and $g = +1$ for a perfectly forward scattering phase function. If a particle scatters all radiation in the backward direction, $g = -1$.

The goal of scattered light studies is to determine g and γ. A serious difficulty in the interpretation of scattered light observations is that one must know something about the spatial distribution of the scatterers. The distribution of the interstellar grains is roughly known for two cases, both of which have been studied in connection with scattered light observations. The first case is the dust distribution in the Galaxy as a whole and the second is in reflection nebulae. Let us consider each of these geometries in turn and see what can be learned about the scattering properties of interstellar grains.

Within a few kiloparsecs of the sun, the galaxy can be represented rather well by a plane parallel distribution of emitters (stars) and absorbers (grains). Viewed on an appropriate scale, both emitters and absorbers can be "blurred out" into continuous distributions of emitting and absorbing material. Both stellar emissions and dust grains decrease in density as one moves out of the central plane of the Galaxy, dropping to about 1/3 of their values in the plane at a height of about 120 pc.

Radiation which has been emitted may be scattered subsequently one or more times so that looking into the Galaxy, one observes both direct star light and a diffuse scattered radiation (often abbreviated as DGR for diffuse galactic radiation). It is the knowledge of the star and dust distributions which makes the Galaxy as a whole suitable for scattered light studies.

In Witt's (1968) observations, the DGR was observed directly by making observations in the Milky Way in fields which are free of stars brighter than twentieth magnitude, and are distributed over various galactic latitudes for the same longitude region. One may then attempt to fit the observed DGR distribution with various models of the galaxy. In particular, one solves the radiative transfer problem for various combinations of g and γ. Aside from the observational scatter, the main difficulty which is encountered here is the nature of the method which is used to solve the radiative transfer problem. Witt (1968) used the Eddington approximation, as did Henyey and Greenstein (1941), and found the observations to be fit best by an isotropic phase function and perfectly reflecting particles; that is, for $g = 0$ and $\gamma = 1$. These observations were subsequently reinterpreted by other authors who have employed other methods for solving the radiative transfer problem for the galaxy model. In particular, van de Hulst and de Jong (1969) have used a method of accounting for multiple scattering by successive integrations of scattered intensities and employing a computer to do the actual numerical computations. They find the albedo to be between .15 and .75, with g between .7 and .4. Mattila (1970) has done a Monte Carlo calculation to determine the surface brightness of a dark nebula in terms of g and γ under the assumption of illumination of the nebula by the Milky Way. He has also reinterpreted Witt's observations of the DGR using the Monte Carlo method to compute the expected surface brightness of a plane parallel galaxy model. Mattila finds g to lie between about .7 and .95 and γ between .5 and .8.

Studies of the DGR serve to indicate that the scattering properties of the interstellar grains in the visible region of the

spectrum are those of a scatterer which has an albedo between .4 and .8 and scatters in the forward direction for visible wavelengths.

Since the extinction is observed to continue to increase as the wavelength decreases (see Figure I), Lillie and Witt (1969) searched for DGR in the ultraviolet. In the visible, the DGR intensity is about .30 of the direct starlight intensity at the galactic equator, so that if γ is the same in the ultraviolet as in the visual region, the DGR should be rather intense. The results of their rocket observations between λ 2100 Å and λ 2800 Å were that γ lies between 0 and .4. More recent work by Witt and Lillie (1972) indicates that γ rises sharply again for $\lambda < 2000$ Å. (See Figure II.)

Having briefly surveyed the scattering properties of interstellar grains as determined from studies using the geometry of the Galaxy, let us turn our attention to another instance in which the problem of geometry of the scatters can be dealt with: reflection nebulae, the objects which are the subject of this paper.

3. The Colors of Reflection Nebulae

Given the knowledge that the extinction efficiency of interstellar grains is wavelength dependent, it is very tempting to try to study the colors observed in reflection nebulae in order to gain some information on the parameters of the particles. The early theoretical work of Henyey and Greenstein (1938) attempted to distinguish between color effects due to particle properties and those due to nebular geometry. The qualitative aspects of the difficulty can be seen as follows: Since blue light is scattered preferentially, the scattered light which originates near the star will be bluer than the illuminating star, while

deeper in the nebula, the starlight which is reaching the scattering grains is already considerably reddened. An additional complicating factor which comes into play is that light which has been scattered may have to traverse part of the nebula to escape into the direction of the observer, in which case it will be reddened. The considerations can become even more complex when one considers phase functions which scatter either toward or away from the observer. If the inverse square dependence of the illuminating starlight causes an inhomogeneous incident radiation field, the approximations needed to solve the radiative transfer problem break down and the color data become even more difficult to interpret.

Considering the difficulties and uncertainties, it is not surprising that colors of reflection nebulae have not provided a great deal of information on the interstellar grains. Observations of the spectra of the Orion and Pleiades nebulae by Henyey and Greenstein (1939) have been interpreted in terms of their theoretical treatment. Under the assumption of an isotropic phase function, they find $\gamma \geq .8$. An important result of these observations is that the extinction by particles in reflection nebulae is proportional to λ^{-1} between 3390 Å and 6450 Å, thus lending support to the assumption that particles in reflection nebulae and the general interstellar medium are similar. Attempts have also been made by Greenberg and Hanner (1970) to combine color and polorization measurements in the study of reflection nebulae. Again, the uncertainties in the geometry make such interpretations very difficult. Perhaps the most important use for color measurements is in discriminating between grain models in which the phase function, albedo, and size distribution are assumed to be known. Some grain models will result in

such particularly strong color distribution characteristics that varying the geometry over the entire range of possible configurations will not fit the observations. (See Greenberg and Roark (1967).)

Having briefly considered the various observations which underlie our ideas about the nature of the interstellar particles, let us now consider in more detail their implications for the surface brightnesses of reflection nebulae.

II. THE THEORY OF THE SURFACE BRIGHTNESSES OF REFLECTION NEBULAE

1. The Hubble Relation

The first observational basis on which it was asserted that the surface brightness of reflection nebulae is due to the reflection of starlight was provided by Slipher (1918). He observed that the nebular and stellar spectra were similar, suggesting the reflection mechanism.

The earliest quantitative work on reflection nebulae is due to Hubble (1922), whose major interest was a test of the idea that the source of luminosity in reflection nebulae was indeed the reflection of starlight. It should be remembered that Hubble's purpose was not the determination of the albedo. In fact, Hubble simply assumed that the albedo was unity and the phase function was isotropic.

An actual reflection nebula may have a quite irregular geometry, be located at a distance which is rather poorly known, and it may not even be known whether the nebula is nearer to or farther from the observer than is its illuminating star. It is thus advantageous to develop observational tests in which as many of these uncertain quantities as possible are eliminated. As will be seen shortly, Hubble's method has this advantage.

To proceed, Hubble made the following assumptions:

1. the inverse square law holds rigorously,
2. all starlight intercepted is reemitted ($\gamma = 1$),
3. the phase function is isotropic,
4. there is no absorption of light between the observer and the star, and

5. the angle of inclination of the nebular surface to the observer's line of sight is random.

In addition, there are several other implicit assumptions being made which will be discussed in the next section.

Figure III shows the geometry of an assumed reflection nebula and the quantities which will enter the discussion. The observer is located at distance R from the nebula. The illuminating star, which is of luminosity L and apparent magnitude m_* as seen from the Earth is located at distance r from arbitrary point P within the nebula. It is an observational fact that $r/R << 1$. The angle from the star to the Earth at point P is α, and the various τ values are optical distances.

An observer who photographs this region will see the illuminating star, the reflection nebula, and a sky background. The maximum apparent angular distance from the star at which the photograph will show the reflection nebula can be limited in one of two ways: first, the nebula might be "dust limited" in that it may have its outer boundary so located that although there is sufficient radiation from the star beyond this point to produce a photographic image, there are no grains to reflect the light. The second possibility is that the light from the star is so faint that when it reaches the most distant regions of the nebula, its reflected intensity is not sufficient to stand out against the night sky background. This may be called the "radiation" limited case. Let us consider the second case and denote by "a" the distance in minutes of arc between the illuminating star and the point at which a photographed reflection nebula's surface brightness just fades into the surface brightness of the night sky. This will of course depend on the particular observing technique, exposure time, etc., but as long as

these are held constant for the set of observations, this is not a problem.

One can then show that a and m_* are related by

$$m_* = -5 \log a + 11.6 + 2.5 \log [\gamma \sin^2 \alpha] - 2.5 \log [(1-e^{-\tau_0})(e^{-\tau_1})] \quad (6)$$

under the assumptions listed above. The details of the derivation of equation (6) in a more general form will be presented in the next section.

2. The Limiting Nature of the Hubble Relation

Equation 6 is in many ways a limiting result, since many effects could act to reduce the value of a. Note, that a dust limited nebula would have a smaller value of a than a radiation limited nebula. Also, the value of a can be reduced by the effects of projection onto the celestial sphere. Equation 6 and the effect of the five assumptions made on its nature as a limiting relationship will be discussed below. For now, it is sufficient for our purposes to note that Hubble determined m_* and a for many reflection nebulae. (See Figure IV.) A correction for the projection effects due to random orientation (i.e., random values of α) was made on the constant in equation 6. The best linear fit to the observations was compared with the lines produced from equation 6 for various assumed values of γ. From this approach, Hubble concluded that the predictions based on the above assumptions of unit albedo and isotropic phase function agreed quite well with the observations. The inconsistency between this conclusion and the more recent

determinations of g and γ was one of the major reasons for undertaking the present investigation.

At this point, the evidence suggesting that the particles composing reflection nebulae and those composing the general interstellar medium are similar and may be summarized as follows:

1. the number of observed reflection nebulae is consistent with the number one would expect on the basis of chance associations between stars and dust clouds,
2. the same extinction law for visible wavelengths seems to hold for both cases, and
3. at least one of the diffuse interstellar features is common to nebular grains and interstellar particles.

These indications, as well as one's tendency to assume the least complicated model until forced to do otherwise, lead one to suspect that the two types of grains are the same. It should be remembered, however, that in many cases reflection nebulae appear to be physically associated with their illuminating stars and it is possible that this circumstance modifies the particles.

Assuming that the particles are in fact the same, it is then of interest to determine why Hubble's relation seems to fit the observations so well, since he assumes unit albedo and isotropic phase function. The forward throwing phase function and γ of about .6 which have been determined for general interstellar particles lead one to expect on rather qualitative grounds that nebulae should appear smaller than the sizes one would find if Hubble's assumptions are correct.

The high surface brightness of reflection nebulae becomes even more perplexing when one considers the limiting nature of the Hubble

relation. Recall that this relation (equation 6) relates the apparent magnitude of the illuminating star, m_*, to the maximum distance from the star at which the nebula is still observable with standard observing conditions (exposure time, emulsion, telescope, etc.). Many effects could operate to reduce the value of $\log \underline{a}$ for a given value of m_*. For example, the nebula might be dust limited or the nebula might be optically thin, shifting a point to the left in Figure IV. Thus, either of these two cases would shift the points to "lower" positions in the diagram. This would result in a downward shift in the least squares line fit from coincidence with the theoretical curve to a position corresponding to an albedo smaller than unity.

Equation 6 can be cast into the form of a limiting relation as follows: inspection of the right hand side shows that $\underline{a}$ has its largest value when $\gamma = \sin^2 \alpha = 1$, $\tau_0 = \infty$, and $\tau_1 = 0$. These are the conditions under which one would expect to maximize the surface brightness on physical grounds. The five assumptions made in deriving equation 6 then lead us to the limiting surface brightness relationship

$$m_* = -5 \log a + 11.6 . \qquad (7)$$

The physical significance of this equation is shown in Figure IV in that no points should lie above the line generated by plotting equation 7, even assuming that the albedo is 1.

The first question which naturally arises is the effect that changing the assumptions used in deriving equations 6 and 7 would have on the surface brightness limit which we expect. The first assumption that the inverse square law holds could only be changed in one way: the intensity received by the nebula is less than one would expect due

to matter between the star and the nebula. This would lead to a decrease in surface brightness. The first assumption of unit albedo can only be changed by reducing γ and thus reducing the surface brightness unless one is willing to consider some additional source of luminosity in the visible region of the spectrum, a possibility which will be discussed later. The assumption that the phase function is isotropic should be changed to an assumed forward scattering if the particles are typical of interstellar particles. In a statistical sense, this could give rise to a nebula being too high on the diagram because the star, assumed now to lie behind the nebula, is made fainter by extinction by the nebula and the nebular surface brightness is higher than would be expected on the basis of an isotropic phase function. However, this assumption also implies that the stars which overstep the Hubble relation all lie behind their nebulae, suggesting that they should have a large color excess. In many cases this is true, but in two of the most dramatic instances, the color excess is nearly zero. These cases are marked B 10 and Ced 201 in Figure IV. Nebula B 10 will be discussed later, but for the present, its main interest to us is that it oversteps the Hubble relation even though the star is in front of the nebula, as evidenced by the fact that the observed color of the star indicates no reddening. Even those instances in which the star shows a color excess do not guarantee that the star is behind the nebula, since the color excess may be due to interstellar matter between the star and the observer. It will be shown in the next section that the Hubble relation is not altered if there is matter located between the nebula and the observer, provided that both nebular light and stellar light suffer the same amount of extinction. Thus, changing assumption 4 concerning

the lack of extinction would not explain the overstepping of the line in the Hubble relation. Finally, the fifth assumption of random orientation between the observer's line of sight and the line between the star and the nebular surface has already been removed by setting $\sin \alpha = 1$.

Many other effects can be noted which could further reduce the observed surface brightness or value of log $\underline{a}$. One such example is the dust limited case, rather than the photon limited case with which we have been concerning ourselves. Considering the many effects which could reduce the surface brightness and the high observed angular dimensions of reflection nebulae, it was felt that a careful reconsideration of the Hubble relation was in order with particular attention to any effect which could raise the surface brightness. To this end, a more general formulation of the Hubble relation was developed.

3. The Derivation of the Generalized Hubble Relation

It is of interest to derive a relationship between the apparent angular extent of a reflection nebula and the apparent magnitude of its illuminating star under the least restrictive set of assumptions possible. To this end, we begin with a set of assumptions and remove them, one by one.

Consider the idealized nebular geometry shown in Figure V. The star is situated a distance r from the patch of nebula and the stellar radiation makes an angle α_i with the normal to the front surface. The observer is located at distance R from both the nebula and the star and his line of sight makes an angle of α_s with the normal to the nebula. Singly scattered photons detected by the observer have been scattered

through an angle θ, where

$$\theta = \pi - \alpha, \tag{8}$$

where α is defined by

$$\alpha = \alpha_i + \alpha_s \quad . \tag{9}$$

If P is any point inside the nebula, denote its perpendicular distance from the front side of the nebula by x. Then τ_1, the optical distance between the front surface of the nebula and P along the line of sight to the star is

$$\tau_1 = kx/\mu_o \ , \tag{10}$$

where k is the extinction per unit distance and

$$\mu_o = \cos \alpha_i \ . \tag{11}$$

We will consider an arbitrary albedo as defined by equation 3 and any arbitrary phase function as defined by equation 4.

With these basic definitions, we will make the following set of assumptions:

1) Only single scattering occurs.
2) Surface brightness contributions from all stars except the nearest star are negligible.
3) The intensity of light from the star falls off as the inverse square of r.
4) The detection limit is determined by photon limitations, rather than dust limitations.

5) The value of r is essentially constant throughout the particular patch of nebulosity under consideration.

6) The patch of nebula under consideration is a plane parallel dust layer of geometric thickness D and optical thickness $kD = \tau_o$, at least for several optical depths in either direction along the nebular surface.

7) There is no obscuring matter between the star-nebula system and the observer.

8) The scattering angles, α, of equation 9 are randomly distributed.

9) Only energy which enters the nebula in the form of visible light can leave the nebula as visible light.

Under these assumptions, the flux at any point P inside the nebula will be the total luminosity of the star spread over a surface area of $4\pi r^2$, but reduced by extinction on the entering the nebula. Thus,

$$I_p = \frac{L}{4\pi r^2} \cdot \exp\left[- \frac{kx}{|\mu_o|} \right],$$

where L is the stellar luminosity. The absolute value sign arises to include those cases for which the star is behind the nebula. If we let σ be the cross sectional area due to extinction contained in a volume of cross section dA and length ds situated at P, the flux intercepted by the grains at P will be

$$I_p \, \sigma \, ds \, dA = I_p \, d\tau \, dA,$$

where it should be noted that σ has units of area/volume. On interaction, the flux will be reduced to γ of its initial value by true absorption

and reemitted into direction α in accordance with the phase function. Thus the energy scattered into direction α is

$$\frac{L}{4\pi r^2} \cdot \exp\left[-\frac{k x}{|\mu_o|}\right] \cdot p(\alpha,\gamma) d\tau dA,$$

where it should be recalled that $p(\alpha)$ is normalized to γ. On its trip to the front surface of the nebula, the energy will be reduced by a factor of $\exp(-kx/\mu)$. The energy emerging from area dA will then travel unhindered to the observer, giving rise to a flux of

$$dI = \frac{L}{4\pi r^2} \cdot \exp\left[-\frac{kx(\mu+|\mu_o|)}{\mu|\mu_o|}\right] p(\alpha,\gamma) d\tau \frac{dA}{4\pi R^2} .$$

The total flux reaching the observer will be the integral along the line of sight through the nebula. Since if we define μ to be $\cos \alpha_s$,

$$d\tau = k \frac{dx}{\mu} ,$$

the total nebular flux will be

$$I_n = \int_0^D \frac{L}{4\pi r^2} \exp\left[-\frac{kx(\mu+|\mu_o|)}{\mu|\mu_o|}\right] p(\alpha,\gamma)\, d\left(\frac{kx}{\mu}\right) \frac{dA}{4\pi R^2}$$

or, dropping the absolute value symbol with the understanding that $\mu_o \geq 0$, and letting $\frac{dA}{R^2} = d\omega'$,

$$I_n = \frac{L p(\alpha,\gamma)}{4\pi r^2} \cdot \left[\frac{\mu_o}{\mu_o+\mu}\right] \cdot \left\{1-\exp\left[-\frac{kD(\mu+\mu_o)}{\mu\,\mu_o}\right]\right\} \frac{d\omega'}{4\pi} .$$

This can be written more conveniently as

$$I_n = p(\alpha,\gamma)\frac{L}{(4\pi r)^2} \cdot G(\alpha)\, d\omega', \qquad (12)$$

where

$$G(\alpha) = \frac{\mu_o}{\mu+\mu_o}\left\{1 - \exp\left[-\frac{\tau_o(\mu+\mu_o)}{\mu\,\mu_o}\right]\right\}, \qquad (13)$$

and $\tau_o = kD$. For brevity, this has been written as $G(\alpha)$ although the actual dependence is on α_i and α_s.

The stellar flux reaching the observer is

$$I_* = \frac{L}{4\pi R^2} \; . \qquad (14)$$

The ratio of nebular to stellar flux is thus

$$\frac{I_n}{I_*} = \frac{p(\alpha,\gamma)G(\alpha)R^2 d\omega'}{4\pi r^2} \; . \qquad (15)$$

If we denoted the angular separation between the star and the most distant patch of nebulosity detected at Hubble's limiting surface brightness by a, then

$$r \sin\alpha = aRc, \qquad (16)$$

where c is the conversion constant from radians to seconds of arc. (This relationship follows from inspection of Figure III and the application of the small angle approximation.) Substituting 16 into 15 yields

$$\frac{I_n}{I_*} = \frac{p(\alpha,\gamma)G(\alpha)\sin^2\alpha\, d\omega'}{4\pi a^2 c^2} \; . \qquad (17)$$

Here, $d\omega'$ is in steradians, but if $d\omega$ is the same solid angle in square seconds of arc,

$$d\omega = d\omega'/c^2 \; , \qquad (18)$$

so that if $d\omega = 1'' \times 1''$ is taken to be our unit of solid angle, substitution of 18 into 17 gives

$$\frac{I_n}{I_*} = \frac{p(\alpha,\gamma)G(\alpha)\sin^2\alpha}{4\pi a^2} \quad . \tag{19}$$

Converting to the magnitude system and adding in a factor of 2(2.5 log 60) to convert a^2 from ' to ", we get

$$m_*-m_n = 2.5 \log[\sin^2\alpha p(\alpha,\gamma)G(\alpha)] - 5 \log a' - 2.5 \log(4\pi) - 2(2.5 \log 60), \tag{20}$$

where m_n is the limiting surface brightness in magnitudes/□" for some standard set of observing conditions.

Thus, the Hubble relation derived under the above assumptions is

$$m_* = m_n + 2.5 \log[\sin^2\alpha p(\alpha,\gamma)G(\alpha)] - 5 \log a' - 11.64, \tag{21}$$

where a' is the angular distance in minutes of arc between the star and the most distant patch of nebula detected.

4. Some Results From the Theory of Radiative Transfer

At this point, it is possible to begin removing the various assumptions, but it is necessary to digress briefly on the method of solving problems in radiative transfer used by Chandrasekhar (1950). The motivation behind turning to radiative transfer is that it is not clear in the original formulation of the Hubble relation what role multiple scattering plays. To modify equation 21 so as to account for multiple scattering will be one aim. The other will be to remove the

the second assumption that only the so-called "illuminating star" contributes to the observed nebular surface brightness. In fact, the reflection nebula must be receiving light from all the stars in the Milky Way. One would expect this contribution to the surface brightness to be small, but it is a possible source of light which could give higher values of albedo than is in fact the case.

Chandrasekhar (1950) requires 126 pages of rather concise mathematics to solve the problem of diffuse reflection from a semi-infinite plane parallel atmosphere composed of particles, having several different phase functions. To attempt even the briefest sketch of his method would carry us far from the topic of interest and would not shed much additional light on the questions at hand. For our purposes, it will be sufficient to remark that he has obtained solutions in closed form for all orders of scattering for plane parallel atmospheres for both the semi-infinite and finite optical thickness cases. Of the phase functions considered by Chandrasekhar, only two will be of concern to us. They are

$$p(\cos\theta) = \gamma \tag{22}$$

and

$$p(\cos\theta) = (1 + x\cos\theta)\gamma \ , \tag{23}$$

where

$$-1 \leq x \leq 1 \ .$$

The first phase function describes an isotropic scatterer and the distribution of scattered radiation for the second case is shown in Figure VI for the two cases x = .5 and x = 1. Note that for positive x values the phase function is primarily forward scattering and for negative x it is backward scattering. To calculate the asymmetry parameter, g, straightforward substitution of equation 23 into 5 gives

$$g = x/3. \tag{24}$$

Since the largest value which x may have is 1, the largest possible g which is available using the phase function of equation 23 is .333. Although this is only about half of the value of g which one finds for general interstellar particles, it is the closest value for which closed form solutions could be found.

Chandrasekhar's closed form solutions to the radiative transfer problems are given in terms of tabulated functions. The tables are generated by numerical solution of one integral equation in the case of a semi-infinite atmosphere and two integral equations in the case of atmospheres of finite optical thickness. The tabulated functions in the former case are called H functions and in the latter case, they are denoted by X and Y functions. It should be noted that H functions and X and Y functions refer to classes of functions rather than a particular set of values as in the sense of sine or cosine functions. Specifically, the H, X, and Y functions must be computed for each different phase function which is considered and will have different sets of numerical values for different phase functions. The practical difficulty of computing these functions depends to a large extent on the complexity of the scattering function. Chandrasekhar (1950) was

able to compute tables of H functions for the phase functions of equations 23 and 24. More recently the X and Y functions have been computed for the isotropic phase function by Sobouti (1963) and by Carlstedt and Mullikin (1966). The freedom of choice of assumed phase function is thus restricted by the availability of the tabulated functions.

For the case of isotropic scattering in a semi-infinite atmosphere, Chandrasekhar (1950, page 124) gives the solution as

$$I(0,\mu,\mu_o) = \frac{\gamma F \mu_o}{4(\mu+\mu_o)} H(\gamma,\mu)H(\gamma,\mu_o) \qquad (25)$$

where F is the incident flux and I is the diffusely reflected flux, both in units of power/solid angle/unit area. I is defined with the unit area oriented perpendicular to the direction of the pencil of radiation, while F is defined with the unit area reduced by the cosine of the angle between the direction of the radiation's motion and the normal to the unit area. Chandrasekhar tabulates the H functions for this problem on page 125. There are two slight differences of notation between this paper and Chandrasekhar's work: first, his ω_o corresponds to our γ and second, I have explicitly exhibited the dependence of H on γ, while Chandrasekhar does not.

For the phase function of equation 23, the solution is

$$I(0,\mu,\phi;\mu_o\phi_o) = \frac{\gamma \mu_o F}{4(\mu+\mu_o)}\{ \psi(\gamma,\mu)\psi(\gamma,\mu_o)-x\Phi(\gamma,\mu)\,\Phi(\gamma,\mu_o)+x[(1-\mu^2)^{1/2} H^1(\gamma,\mu)]$$

$$\cdot[(1-\mu_o^{\,2})^{1/2} H^1(\gamma,\mu_o)] \cos(\phi_o-\phi)\} . \qquad (26)$$

The solution and the tables of required functions are on page 141 of

Chandrasekhar's Radiative Transfer. The superscripts on the H functions distinguish them from the H functions for isotropic scattering. Here, ϕ and ϕ_o are azimuthal angles measured about the normal to the nebular surface. As usual, a zero subscript denotes incidence and no subscript denotes scattering angle. Both ψ and Φ are tabulated functions.

On page 209, Chandrasekhar gives the solution for the diffusely scattered and transmitted flux for an atmosphere of finite optical thickness and isotropic scatterers as

$$I(o,\mu) = \frac{\gamma\,\mu_o F}{4(\mu+\mu_o)}\,[\,X(\gamma,\mu,\tau_o)\,X\,(\gamma,\mu_o,\tau_o) - Y(\gamma,\mu,\tau_o)\,Y\,(\gamma,\mu_o,\tau_o)] \tag{27}$$

and

$$I(\tau_o,-\mu) = \frac{\gamma\mu_o F}{4(\mu+\mu_o)}\,[\,Y(\gamma,\mu,\tau_o)\,X\,(\gamma,\mu_o,\tau_o) + X(\gamma,\mu,\tau_o)\,Y\,(\gamma,\mu_o,\tau_o)], \tag{28}$$

where I have rearranged terms slightly. It should be noted that the diffusely transmitted flux term, $I(\tau_o,-\mu)$, does not include the radiation which has suffered no interaction; this radiation has the original direction of travel and is reduced in intensity by a factor of $\exp(-\tau_o/\mu_o)$ from its intensity on entering the nebula.

Figures VII and VIII show the γ dependence of the X and Y functions for selected values of τ_o and μ .

5. The Correction for Illumination by the General Stellar Field

We are now ready to consider the effect of illumination by the general stellar field. To do this, consider all stars except the

"illuminating star" as spread uniformly over the surface of a sphere and denote the surface brightness of the sphere by I_o. We then may compute the intensity which will be reflected due to light incident from some angle, α_i, and integrate over all angles of incidence for some fixed angle of observation, α_s, thus determining the contribution to the surface brightness due to illumination from the general stellar field.

Figure IX shows the geometry of the situation under consideration. Light is incident from a strip of area $A(\alpha_i)$ given by

$$A(\alpha_i) = (2\pi \sin \alpha_i)\, d\alpha_i \quad .$$

The weighting factor for this strip is the strip area divided by the total area of a hemisphere. The hemisphere is replaced by a sphere for cases in which the nebula is of finite optical thickness. The weighting factor is then

$$W(\alpha_i) = 2\pi \sin \alpha_i \, d\alpha_i/2\pi = \sin \alpha_i \, d\alpha_i = d\mu_o$$

Hence, the integration is carried out by taking equal steps in μ. Because the functions involved do not change rapidly with angle, the integrations were done with only five steps. It was found that the difference between a five and a ten step interval amounted to only two parts in a thousand, a small error compared to the other uncertainties in the following calculation. The integral being evaluated is of the form

$$I = \int_0^1 I(o,\mu,\mu_o)\, d\mu_o \quad .$$

Because the emergent flux scales linearly with the incident flux, the calculations can be done for unit incident flux and scaled for any value of surface brightness of the assumed uniform hemisphere.

For finite τ_o, the front and rear surface intensities are added together to account for the fact that both sides of the nebulae are being illuminated.

Figure X shows a plot of the relative importance of the light entering from the various angles corresponding to the various μ_o values for a semi-infinite isotropically scattering atmosphere for $\mu = 1$. Physically, the total surface brightness will be the area under the curve and will be in units of incident flux. As might be expected, the reflected surface brightness is strongly dependent on the value of γ which one assumes the particles to have. For γ near unity, multiple scattering provides more opportunity for the incident photon to escape again, while for lower albedo, the single scattering is smaller by a factor of γ and the contribution from radiation which has been scattered n times is reduced by a factor of γ^n.

Integrations of the type just described were carried out for the isotropic phase function for $\tau_o = \infty$, 2, 1, and .6. The calculations for finite optical thickness only include the diffusely transmitted flux, since the directly transmitted flux is visible on a photograph as a star and would be avoided in searching for the most distant patch of luminosity on a photograph. (It must be remembered that the uniform hemisphere or sphere is only an approximation.) Similar calculations were made for the phase function of equation 23 with g = 1/3, corresponding to x = 1. However, due to the unavailability of tables of the X and Y functions, these calculations were only possible for $\tau_o = \infty$. Table I gives the values which were thus derived for the expected surface brightness due to illumination from the general stellar field (hereafter abbreviated GSF). Two points should be noted: first, the values

for finite τ_o cases in which g = .333 were taken to be the same as the values obtained for the isotropic case. This can be justified to some extent by noting that in the finite case the nebula is illuminated from both sides and the extent to which light is forward (or backward) scattered by one surface is about the same extent to which it is forward (or backward) scattered by the opposite side. This argument becomes less satisfactory as the albedo becomes smaller, but for small albedo values the correction becomes small anyhow. Second, the calculations were repeated with $\mu_\odot$ = .7 (corresponding to $\alpha_\odot \simeq 45°$) and the changes in surface brightness were less than 10% in all cases.

Since the GSF correction coefficients of Table I have the physical meaning of the fraction of incident GSF light which is diffusely reflected by the nebula, we have an opportunity to check the reliability of the calculations to this point. A dark nebula is a cloud of interstellar grains which is not near enough to any one star to shine by reflection, but such nebulae should have about the same surface brightness which is being calculated here, since such a nebula must be illuminated by the GSF.

Mattila (1970 b) has measured the surface brightness of the Coalsack dark nebula, one of the most prominent of all dark nebulae. In addition to the surface brightness of the Milky Way, Mattila also had to include the effect of two bright stars relatively near to the Coalsack. He uses a value of $I_o = 69\ S_{10}/\square°$ (tenth magnitude stars per square degree) for the average surface brightness due to the GSF plus the two stars. This value is for the standard blue filter of the UBV

system. Neglecting the two stars would have reduced his value to 66 $S_{10}/\square^\circ$ in the blue. In the visual, I_o was taken to be 118 $S_{10}/\square^\circ$. These values were taken from the photoelectric photometry of Elsässer and Haug (1960) and the integrated starlight values of Roach and Megill (1961). Assuming infinite τ_o and $\gamma = .6$, Table I indicates that about 10% of the GSF should show up as surface brightness for a dark nebula, corresponding to about 7 and 12 $S_{10}/\square^\circ$ in the B and V bandpasses, respectively. Mattila actually observes about 50 and 80 $S_{10}/\square^\circ$ for the Coalsack and about 14 and 26 $S_{10}/\square^\circ$ for a dark nebula in the constellation Libra.

While the agreement is not extremely good, there are several systematic effects which operate in the direction of making the calculated values too small. In particular, the approximation of a uniform sphere as the source of illumination is certainly not reliable, for most of the surface brightness incident on the Coalsack ($b^{II} = 0^\circ$) comes from the band of the Milky Way. Since we are also essentially in the plane of the Galaxy, the large values of the function $\mu_o/(\mu+\mu_o)$ for light reflected to the Earth from the plane of the galaxy should actually be weighted more heavily. The uniform sphere model weights all points equally, thus reducing the calculated value of the surface brightness. The magnitude of the GSF correction can at least be taken to be correct.

How can these results be incorporated into the Hubble relation? The term m_n in equation 21 refers to the limiting magnitude/$\square''$ which will just blacken a photographic plate. This has been interpreted to be due exclusively to surface brightness from the illuminating star, but we will now recognize that the intensity corresponding to this surface brightness limit, I_{lim}, is the sum of two terms:

$$I_{lim} = I_S + I_{GSF} ,$$

where the GSF implies general stellar field and S implies nebular surface brightness due to the illuminating star. If we denote the GSF correction coefficients of Table I by $\Delta(\gamma,\tau_o)$ and the average surface brightness of the Milky Way averaged over a uniform sphere by I_o,

$$I_{lim} = I_S + I_o \cdot \Delta(\gamma,\tau_o) \quad .$$

Physically, for the same limiting surface brightness, the star will now make the nebula appear larger, since the two sources of surface brightness are now adding. Rearranging the last equation, dividing both sides by I_{lim}, and converting to the magnitude system, we find

$$-D \equiv m_{lim} - m_S = 2.5 \log \left(\frac{I_{lim}}{I_{lim} - I_o \cdot \Delta}\right). \quad (30)$$

D is thus a positive number which is to be added to the right hand side of equation 21 to correct for GSF illumination. Note that when $I_o\Delta$ is not zero, $D > 0$, and equation 30 can be written

$$m_S = m_{lim} + D \quad . \quad (31)$$

In this form it is clear that D "assists" the illuminating star in causing plate blackening by reducing the magnitude per solid angle which the star must provide for a fixed limiting magnitude. It should be noted that if $I_o \cdot \Delta \geq I_{lim}$, equation 30 becomes unphysical. This simply corresponds to the case in which the component of surface brightness of the reflection nebula due to the GSF is brighter than the detection

limit and all nebulae become visible on the plate, even in the absence of an "illuminating star".

Before leaving the topic of the GSF correction, it is of interest to compute the importance of this correction for reasonable assumptions. Hubble gives his plate limit as about $23.25^{m}/\square''$, corresponding to 65 $S_{10}/\square^{\circ}$ (photographic). Taking I_0 as 66 $S_{10}/\square^{\circ}$ (B value, but close enough for the rough illustrative calculation), consulting Table I shows that Δ may range from .5 to .05 for reasonable γ and τ_0 values, leading to I_{GSF} values which are from 5% to 50% of the detection limit.

6. The Correction for Higher Order Scattering

Much the same technique as that discussed in the previous section for the general stellar field correction may be used to include multiple scattering. Again, Chandrasekhar's exact solutions as given in equations 25 - 28 were calculated for constant γ, μ_0, and τ_0, yielding values of $I(\mu)$. Since our aim was to correct the single scattering result of equation 21 for higher order scattering, for each exact calculation of $I(\mu)$ described above, the intensity due only to single scattering was calculated and plotted on the same graph. Figure XI shows the results of several such sets of calculations.

The singly scattered flux is given by Chadrasekhar (1950, page 146) as

$$I^{(1)}(0,\mu,\phi\ ;\ -\mu_0,\phi_0) = \frac{F\mu_0}{4(\mu+\mu_0)}\, p(\mu,\phi,-\mu_0,\phi_0). \qquad (31)$$

Since the phase function is normalized to γ (see equations 22 and 23), the singly scattered flux scales linearly with γ.

The basis of the multiple scattering correction technique is the following empirical observation: inspection of the plots of Figure XI shows that the difference between the exact and single scattering solutions is a constant to a good approximation. That is, for a fixed set of γ, τ_o, g, and μ_o values, it is approximately true that

$$I(\gamma,\mu,\tau_o,g) = I^{(1)}(\gamma,\mu,\tau_o,g) + C(\gamma,\tau_o,g) \quad , \qquad (32)$$

where the multiple scattering correction coefficient, C, must be empirically determined for each combination of the values of γ, τ_o, g, and μ_o. Mattila (1970 a) has solved the radiative transfer problem for spherical nebulae using the Monte Carlo technique. He presents some plots of single and multiple scattered intensity and inspections of his plots shows that the empirical relationship of equation 32 also holds for other geometries.

The actual determination of the values of C involves less work than a casual inspection of equation 32 might suggest. It was found that C was very insensitive to μ_o and the lack of tabulated X and Y functions made it impossible to determine the C values for finite τ_o values when g = .33.

The lack of dependence of C on both μ and μ_o is easy to understand: C is a measure of the intensity of the radiation which has undergone more than one scattering and thus, the original directionality which the incident beam of light had has become blurred by

several scatterings. This multiply scattered radiation would be expected to be rather isotropic.

The values of the C's were determined by measuring the distance between the exact and single scattering curves and expressing the result as a fraction of the incident intensity, taken as unity in all cases. In those cases in which τ_o is finite, the single scattered intensity (see equation 31) must be multiplied by $1 - \exp[-\tau_o]$ to scale the single scattered intensity to τ_o. In most cases this was not difficult, but inspection of the plots of Figure XI shows that the two curves are not always the same shape. In these instances an estimate of the average difference between the two curves was made.

Table II lists the values of the multiple scattering correction coefficients which were used. The values were slightly different for the front and rear surfaces in the case of finite τ_o values. A rear surface is of course meaningless for a semi-infinite atmosphere.

Denoting the values listed in Table II by $C(\gamma, \tau_o)$, we may now see how to modify equation 21 in order to correct for multiple scattering. The physical interpretation of the C values is that they are the intensity of the multiply scattered light, measured in terms of the incident flux. The correct expression for the nebular surface brightness can then be written as (see equation 14)

$$I_n = \left[\frac{LpG}{4\pi r^2} + \frac{LC}{4\pi r^2} \right] \frac{d\omega'}{4\pi} , \qquad (33)$$

where again L is the stellar luminosity in the visual and r is the distance between the star and the patch of nebulosity under consideration. Note that the second term of equation 33 does not contain γ, p, or G since these terms have already been included in the numerical value of C by virtue of its empirical determination.

Exactly the same steps which take one from equation 16 to equation 21 can be followed starting with equation 33 leading to the result

$$m_* = m_{lim} + D - 5 \log[a'] + 2.5 \log [\sin^2\alpha \{G(\alpha) + C\}] - 11.64$$

here, C is multiplied by $\sin^2 \alpha$ to correct for projection effects due to inclination of the line between the star and the nebula to the line of sight. Comparing this equation with equation 21 shows that the correction for illumination by the GSF has also been incorporated into this equation. The term m_n has now been replaced by $m_{lim} + D$, accounting for the fact that the plate limit can be reached by a combination of illumination from both the illuminating star and the GSF.

There remain two corrections which must still be applied to this equation, both of which are of a statistical nature. To this point, everything has been done assuming that we know the angle α, when in fact we may at best assume a statistical distribution of angles. This is discussed below, but one point which is worthy of note now is that it is as likely that the star will lie behind the nebula as that it will lie in front of it. In the latter case, no modification in the last equation is necessary, but in the former, the stellar flux reaching the observer would be reduced by a factor of $\exp[-\tau_o/\mu_o]$.

Converting this expression to the magnitude system, this correction can be incorporated into the last equation to give

$$m_* = m_{lim} + D - 5 \log [a'] + 2.5 \log [\sin^2 \alpha \{p(\alpha,\gamma)G(\alpha) + C\}] - 11.64$$
$$- \{ \frac{\mu_o + |\mu_o|}{2\mu_o} \} \cdot 2.5 \log [\exp(-\tau_o/\mu_o)]. \quad (34)$$

The term in μ_o multiplying the last logarithm expression is simply an artifice, so designed that it is zero for $\mu_o \leq 0$ (star in front) and unity for $\mu_o > 0$. In practice, the sign of μ_o was tested in a program and the last expression added in or not, as appropriate.

7. The Computational Technique for Determination of γ

With equation 34 as a starting point, we can now devise a computational technique for determining the albedo for any assumed phase function for which it is possible to determine the correction terms C and D. To do this, we note that the least squares fit to the observed m, log a diagram produces a relationship of the form

$$m_* = H_o - 5 \log a'. \quad (35)$$

(The details of the least squares fit are discussed below.) Subtracting this last equation from 34 leads to

$$q = m_{lim} + D(I_o,\Delta) - H_o - 11.64 + 2.5 \log [\sin^2\alpha \{p(\alpha,\gamma)G(\alpha,\tau_o)$$
$$+ C(\alpha,g,\tau_o)\}] - \{ \frac{\mu_o + |\mu_o|}{2\mu_o} \} \cdot 2.5 \log [\exp(-\tau_o/\mu_o)].$$
$$(36)$$

The condition that the theoretical and observational equations agree is satisfied when $q = 0$.

Since the details of the geometry of any particular reflection nebula are unknown and since equation 35 is based on the observations of many nebulae, it is obvious that we must average equation 36 over all possible angles. The proper method of angular averaging has been a subject of some confusion in the literature. In his original discussion of the problem, Hubble (1922) gives a very brief discussion of the calculation of the angular correction factor. His entire discussion of the correction (taken from page 410 of his paper) follows:

> "Assuming a random distribution of directions from star to nebulosity, the mean $\underline{a}$ observed, projected on a plane perpendicular to the line of sight, should be less than the true $\underline{a}$ by the factor $\pi/2$. This difference can be corrected by increasing $\underline{m}$ by $5 \log \pi/2 = .98$."

Zanstra (1927) recalculated the projection correction factor by considering the star to be situated at the center of an imaginary sphere of radius $\underline{a}$ and the patch of nebulosity to be of area $d\sigma$. Assuming all angles, α, between the line of sight and the line connecting the star and the patch of nebulosity to be equally probable, the distance seen projected on the sky will be on the average

$$\langle a \rangle = \frac{\oint a \sin \alpha \, d\sigma}{\oint d\sigma} = \frac{\pi a}{4} .$$

Thus,

$$5 \log \langle a \rangle = 5 \log a + 5 \log \frac{\pi}{4} = 5 \log a - .52 .$$

If the range of integration is restricted to lie between $0 \leq \alpha \leq \frac{\pi}{2}$, Hubble's value of the correction of -.98 results. Neither of these authors has attempted a detailed treatment of this problem. Certain selection effects are probably inherent in the data in the sense that nebulae for which α is small are more readily observed than are those nebulae for which α is large. This is most readily seen by consulting Figure X. The surface brightness is seen to decrease significantly for those angles of observation for which $\mu = \cos \alpha_s$ is small. An additional complication is introduced by the fact that the surface brightness does not depend on α, the sum of the angles of incidence and scattering, in a simple fashion, as inspection of equations 25 - 28 reveals.

For the above reasons it was felt that the best approach to the problem of the angular averaging necessary in equation 36 was a numerical computation. The method which was adopted was to start by assuming a phase function (from the limited choice of two) and an optical thickness τ_o of .6, 1, 2, or ∞. A value of γ was then also assumed. This then specifies the values of the correction constants C and D of equation 36. The argument of the logarithm was then computed by the expression

$$\int_o^{\pi} d\alpha_i \int_o^{\pi/2} d\alpha_s \left\{\left[\left(\frac{\mu_o}{\mu + \mu_o}\right) p(\alpha) \exp\left[-\tau_o \left(\frac{\mu + \mu_o}{\mu \mu_o}\right)\right] + C(\gamma, \tau, \mu)\right] \sin^2 \alpha\right\} \Big/ \int_o^{\pi} d\alpha_i \int_o^{\pi/2} d\alpha_s . \qquad (37)$$

In practice, this was done by averaging the values of the arguments over all values of incidence and scattering in 10° steps. The value of q was then computed. The value assumed for γ was then changed and the process was repeated. This was carried out on the University of Toledo's IBM 360-44 computer, which printed a table of γ and q. The γ value corresponding to $q=0$ was then determined by interpolating the table. These results are discussed in the next section.

III. THE IMPLICATIONS OF THE CALCULATIONS

1. The Results of the Calculations

With the formalism which has just been presented, it is only necessary to choose the proper values of the input parameters in order to compute the value of γ (for an assumed phase function). For assumed input parameters, the correct γ value is that value for which q of equation 36 is zero, corresponding to agreement between theory and observation. The most obvious choice of input parameters is the set of values which Hubble (1922) used. This was done and Table III lists the values used by Hubble for m_{lim} and H_o, the limiting surface brightness in magnitudes/□" and the magnitude axis intercept of the least squares fit to the observed points on the m, log a plot, respectively.

Hubble's (1922) least squares fit to his observations is actually given by

$$m + (4.90 \pm .13) \log a = 11.02 \pm .10. \qquad (38)$$

Since there is a theoretical reason to expect that the coefficient of the logarithm term should be 5 and since 5 does fall into the range of the uncertainty, Hubble chose to force a fit with the coefficient 5. He finds

$$m + 5 \log a = 11.10 \qquad (39)$$

to differ from the values given by equation 38 by less than a tenth of a magnitude over the entire range of 14.2 magnitudes covered by his observations.

In addition to the values given by Hubble, the more recent and extensive work of Dorschner and Gürtler (1966) was consulted for

input parameter values. Hubble (1922) considered 82 nebulae in the photographic region, while Dorschner and Gürtler (1966) consider 196. Dorschner and Gürtler determined values of log a from studies of the Palomar Sky Survey prints, assuring that the material is reasonably uniform and complete. For both the red and blue prints of the PSS, least squares fits to the data gave results for the coefficient of the logarithm term such that it can be taken to have the theoretical value of 5 and still lie between the regression curves to the accuracy with which they can be specified.

Table III summarizes the results of the model calculation. Here, I_0 is the GSF average intensity in $S_{10}/\square^o$, m_{lim} is the plate limit in $m/\square''$, H_0 is the intercept on the m axis of an m, log a plot, and τ_0 is the optical thickness normal to the plane of stratification.

The uncertainties given in Table III are about ± .05, as determined by varying each of the input parameters by its maximum uncertainty and in such a direction as to make γ as large (or small) as possible. The empirical determination of many of the correction coefficients discussed in the previous section necessitated the estimation of their uncertainties in a rather rough fashion. Inspection of Figure XI led to the estimate of the uncertainty of ± 30 % for both C and D.

The value of γ which one assigns to the particles of reflection nebulae is now seen to depend on the value which is assumed for the optical thickness, τ_0. The best technique to follow at this point would be to take an average of the values thus determined, weighted according to the distribution of optical thicknesses. However, very little is known about this distribution. An upper limit to the thickness is probably about 3, a value determined by Lynds (1965) for a high latitude dark

nebula and by Mattila (1970 a) for the Southern Coalsack. The lower limit of the optical thickness is probably set by selection effects, and is probably not too far from $\tau = .6$. The "average" optical thickness is probably between 1 and 2.

Even if we consider the albedo values determined for $g = 0$, they are seen to run somewhat higher than the upper limit as determined by the DGR studies. Note that as g is increased to 1/3, the albedo tends to increase slightly. It is likely that when g is increased still further, γ will also increase, although to what extent is difficult to estimate.

Although the more detailed treatment of the Hubble relation has reduced the value of the albedo, the values of γ obtained from these calculations are high in comparison with the values as determined for interstellar particles by other means. It is important to remember that the particles composing reflection nebulae may not be typical of general interstellar particles, but this is a conclusion which should be drawn only after all other possibilities have been considered. The search for possible sources of the high observed surface brightness (other than the explanation that the value of γ is near unity) should naturally begin by again considering how changes in the assumptions made in deriving equation 36 would affect our results.

2. An Examination of the Assumptions Underlying the Theory

Nine assumptions were listed at the beginning of the discussion of the generalized Hubble relation. The systematic effects of the first two assumptions presumably have been eliminated by the corrections for multiple scattering and illumination by the GSF. It was argued in Section II that if the intensity of light falls off more rapidly than

r^{-2}, the effect will be to underestimate γ. It was also argued there that γ will be underestimated if the nebula is dust limited, rather than photon limited. Thus, changes in the third or fourth assumptions will only raise the values of γ given in Table III. Changing the assumption of a constant value of r for the patch of nebulosity under consideration can also only raise γ. If we choose r to describe the distance from the star to the center of the patch of nebulosity, changing assumption 5) implies that the side of the patch nearer to the star will receive more light than the other half of the surface of the patch. To first order, these differences will cancel. To second order, due to the r^{-2} dependence, the more distant section will receive less light than we are assuming, thus being less bright and hence, reducing the value of γ which we will determine.

The relationship between surface brightness and the sixth assumption of a uniform, plane parallel geometry (at least for several optical thicknesses along the nebular surface) is more difficult to determine. Certainly this condition will not ever be exactly fulfilled, but it is rather hard to imagine how it would be possible to cause the surface brightness to increase over the value predicted by the plane parallel model. Mattila (1970 b) presents plots of his Monte Carlo calculation results for single and multiple scattering which indicate that the multiple scattering correction and fraction of total light reflected from a spherical nebula are nearly the same as the values determined for a plane parallel nebula of the same τ_0, γ, and g. Thus, one is not led to suspect any major increase in the observed surface brightness due to an irregular geometry.

The seventh assumption (no obscuring matter between the star-nebula system and the observer) must be examined with respect to two cases. The first possibility is that all of the material lies uniformly distributed in the line of sight, obscuring both star and nebula to the same extent. It has been shown by Cedarblad (1946) that this condition leaves the form of the Hubble relation unaltered. If the distribution of obscuring material is such that either the star or nebula is obscured more heavily, the observed surface brightness can be either higher or lower than predicted by the Hubble relation. In the construction of a Hubble plot of the type of Figure IV, there is a selection effect operating which will tend to make the nebulae appear too large if the interstellar extinction varies rapidly over the region of the celestial sphere covered by the star and the nebula. To visualize the origin of this effect, consider a star situated in front of a plane parallel nebula. With zero extinction, one would see the star at the center of a nebula whose surface brightness faded to the same extent along any radial direction until it reached the surface brightness of the night sky. However, the introduction of rapidly varying extinction over this field of view would result in some random value of extinction for the star and a distribution of extinction for the "edges" observed for the nebula. The patch of nebulosity experiencing the lowest extinction will be selected by an observer for his determination of log a. This leads to an overestimate of log a for every case except that for which the extinction suffered by the star is smaller than the extinction experienced by light leaving every point of the detectable "edge" of the nebula. The magnitude of this effect is very difficult even to estimate. Münch (1952) gives the number of interstellar clouds one encounters in a one

kiloparsec line of sight in the galactic plane as about 7. Assuming a typical reflection nebular distance to be about a kiloparsec and the average interstellar cloud to be situated about 500 parsecs away and 1 parsec in diameter, this cloud has an angular extent of about 6 ' , to be compared with typical values of 1 ' to 10 ' for reflection nebulae. The accuracy of the available data do not justify a detailed statistical analysis of the correction to be applied for this effect. Although this correction might be important in the instance in which a large number of nebulae are being considered, there are several individual instances in which the Hubble relation is overstepped, even in its limiting form by nebulae whose illuminating stars have colors which indicate that they are not reddened by any obscuring matter.

The second case related to assumption 7 (no obscuring matter between the star-nebula system and the observer) is the possibility that the star is situated within the nebula. (The possibility that the star is behind the nebula has already been accounted for in the last term of equation 36.) This possibility is quite difficult to treat in even an approximate manner. However, it can be seen that the effect of such a geometry will be to cause one to assign a value to γ which is too low. This must be the case, since we could regard the nebular material between the patch of nebula which we are considering and the star as additional extinction, the effect of which is to cause the intensity of the star light to decrease more rapidly than r^{-2}. This effect has already been considered above, where it was shown that this would cause an underestimate of γ.

The eighth assumption, namely that the distribution of angles of inclination between the observer's line of sight and the line

connecting the star and the nebula is random would appear to be sound. However, there is the possibility of selection effects which might affect the Hubble diagram. When a reflecting surface which reflects uniformly in all directions is viewed at larger and larger angles to its normal, the projection effect will increase its surface brightness. This is so because the amount of energy radiated in a particular direction remains the same, but the area from which it appears to come decreases. (Inspection of plots of reflected intensity as a function of observation angle shows that the approximation of equal intensity in all directions is reasonably good.)

Since this is a possible explanation for the high albedo, it is necessary to estimate its importance. This is rather difficult to do accurately, but some indication of the magnitude of the effect can be obtained by incorporating a rough selection effect into the model used to determine the value of γ. This was done by repeating the calculation with the additional feature that all terms for which the angle of observation was more than 45° away from the normal were counted twice. This then reduces the value of γ by about .05 to .07, depending on the phase function and optical thickness assumed. However, even when this selection effect is included, the albedo is still higher than the value obtained by DGR studies.

Examination of the assumptions to this point indicates that changing any of them will result in an increase in the albedo with the exception of assumption 8), and an estimate of the magnitude of this effect indicates that it is probably too small to explain the high albedo determined by the Hubble relation. Thus, we are led to consider the possibility that some of the energy leaving the surface of a reflection nebulae as visible light entered the nebula in some other form.

3. The Possibility of Fluorescence

Since the determination of the albedo of the particles appears to give a value somewhat higher than that determined for other interstellar particles, one is led to consider the possibility that there might be another source of surface brightness which has not been considered in the calculation. One such possibility is fluorescence. The idea that fluorescence might occur in reflection nebulae is not new.

Observations of the reflection nebula B 10 lead Struve and Swings (1948) to propose fluorescence as a possible source of additional surface brightness in reflection nebulae. Struve and Swings were led to investigate this nebula in detail when they noted that it dramatically oversteps the Hubble relation (see Figure IV). The illuminating star is more than 7 magnitudes fainter than the value which one would expect from the Hubble relation. Struve and Swings consider several possible explanations, such as illumination of the nebula by another star, but are not satisfied that the difference can be explained. In particular, the reflected spectrum resembles the spectrum of the star assumed to be the illuminating star. The illuminating star shows strong emission lines of hydrogen and Ca II and some He I. The nebular spectrum shows these same lines, but the lines are weaker in relation to the continuum than they are in the star. This, combined with the unusually large angular extent for a nebula illuminated by such a faint star, led Struve and Swings to propose fluorescence as a possible mechanism for surface brightness. Since many materials in the laboratory are known to fluoresce under irradiation by far ultraviolet light, continuous fluorescence may be sought as a possible cause of high

surface brightness in reflection nebulae, and the consequent overestimate of the albedo of nebular particles.

Further circumstantial evidence on the possibility of fluorescence exists. Numerous observers have reported continuous fluorescence on the lunar surface. Link (1961) has investigated the relative depth of solar lines and the same lines as observed in the lunar spectrum. He finds the reflected lunar lines to be less deep in the relation to the continuum than the same lines in the solar spectrum. There are indications that this phenomenon may not be due to excitation by ultraviolet light, for the lunar fluorescence can be correlated to changes in the solar constant and is observed to lag from one to two days behind corresponding solar changes. This suggests the possibility that the energy for the fluorescence may arrive at the lunar surface in the form of high velocity charged particles from the sun.

Blair and Edgington (1968) have studied the spectra of a number of minerals which are bombarded with 146 MeV protons. Figure XII shows reproductions of some of their spectra for certain minerals. In many cases, Blair and Edgington report significant enhancement of fluorescence at low temperatures (liquid nitrogen temperature). Among these minerals is enstatite, a material found in meteorites. Similar work has been reported by Derham and Geake (1964), although their work was confined exclusively to enstatite. This particular mineral is of some interest now, for it is being considered as a possible constituent of interstellar particles. (See Krishna Swamy, 1972). These spectra were taken when the source was bombarded by 40 KeV protons.

The experiments discussed above were both conducted using particles to excite the fluorescence. However, as pointed out by

Becker (1969), the fluorescent spectrum is frequently independent of the source of its excitation. Spectra shown by Becker (1969) indicate that many organic molecules fluoresce under UV excitation. These molecules frequently have quite broad emission features.

The final piece of circumstantial evidence for the possibility of fluorescence which we will consider is the form of the curve of albedo as a function of wavelength (see Figure II). The dip in the albedo in the ultraviolet indicates that the particles must be absorbing strongly in this region and while it is possible that the energy goes into heating the particle, there is also a possibility that fluorescence may occur.

4. The Spectrophotometric Work of Witt and Rush

Any significant contribution to the surface brightness of reflection nebulae by a mechanism which involves discrete emission lines can be ruled out because earlier observers, such as Slipher (1918) noted the close similarity between spectra of nebulae and illuminating stars. It should be possible to detect the presence of continuous fluorescence in reflection nebulae by comparing the spectra of the illuminating stars with the nebular spectra. The lines in the stellar spectrum should appear deeper in comparison to the continuum, since fluorescence would raise both the intensity at the line center and in the continuum by equal amounts.

In order to detect such possible fluorescence, Witt (see Witt and Rush, 1971) has made observations on the spectra of several reflection nebulae and their illuminating stars. Spectrograms were obtained of the night sky before and after the nebular observations. Densities of the stellar, sky, and nebular spectrograms were measured point by point and put on computer cards. To correct for the sky background, the sky

observations were averaged and subtracted from the nebular results, point by point. In order to reduce noise, the results of several observations of the same nebula were aligned and averaged. Stellar spectra were similarly averaged. Then the ratio of the nebular intensity to the stellar intensity is computed for each wavelength. If the only source of nebular surface brightness is pure reflection, the result of plotting these ratios as a function of wavelength should be a straight line. Fluorescence would manifest itself as a sharp increase in the value of the ratio each time an absorption line was crossed. The results are shown in Figure XIII. NGC 1435 and NGC 2068 are reflection nebulae and the points were determined at each of the hydrogen absorption lines. The ordinate is fluorescent intensity, Φ, in units of the reflected continuum intensity. The scattered light controls are 15 Sextantis and ξ^2 Ceti, two stars which are free of nebulosity. These were included as a check of the reliability of the technique.

The results of these observations indicated that from 10% to 30% of the reflected continuum intensity appeared as an additional continuous contribution. However, what might otherwise be a definitive result is made dubious by the presence of a photographic complication. To see the nature of the difficulty, consider Figure XIV. In A we see a plot of the intensity, I, of the reflected light as a function of distance, r, from the illuminating star for both line and continuum. In general the intensity decreases with increasing r. Both the continuum and the line center intensities (C and L) are shown with linear gradients, although the effect operates with any gradient. In B we see the photographic characteristic curve, which relates the density of the exposed and developed plate to the total intensity which struck the plate

(reciprocity effects are not our concern at the moment.) Note in particular the existence of a linear region for large intensities, followed by a flattening at lower intensities, commonly called the toe of the curve. In C we see what the density of the photographic plate will look like after the plate is exposed. The continuum will still be linear (or have the same shape that it originally had) because in this region of the characteristic curve (B) the transformation or mapping from log I to D, the density, is linear. However, at the lower intensity at which the line center is being exposed, the transformation from log I to D is non-linear, resulting in a distortion of the type shown schematically in C. The result of this is that when one makes a microdensitometer tracing by aligning the slit parallel to the spectral lines, he is effectively determining the intensity at a different r value in the line than in the continuum. This can be seen by noting that in C, the value of r which corresponds to the center of a rectangle having the same area as the area under the continuum curve is the central dotted line. However, for the curve marked "L", the area centroid is shifted to the left. Hence, it is not accurate to compare the two intensities as thus determined, since they correspond to different effective distances from the illuminating star. The question of whether or not this effect is large enough to invalidate the conclusion is difficult to answer definitely. All values in Figure XIII were determined by averaging two or more spectra of the same object to reduce noise, the only exception being ξ^2 Ceti, which is the result of only one observation. It should also be remarked that this spectrogram was not well exposed, so that if the effect described above is a problem, it would be expected to be most severe here. It would thus seem that no really firm conclusion

regarding fluorescence in the interstellar grains can be drawn at this point. However, it would also seem that available evidence suggests that a further investigation in this area is warranted. The first step in this direction was to include fluorescence in the theoretical treatment of a nebular surface brightness in order to establish whether or not the possible fluorescent intensities of Witt and Rush (1971) are sufficient to reduce γ to the value obtained by other means.

5. The Inclusion of Fluorescence in the Theory

With the formalism which has been developed in Section II, it is a fairly simple matter to include fluorescence. Let us assume that the fluorescent light is emitted isotropically. Let us then define a fluorescence parameter, Φ, as the ratio of the component of surface brightness due to fluorescence to the component of surface brightness due to reflection. Inspection of equation 36 shows that the reflected surface brightness is given by the terms

$$\sin^2\alpha \quad \{p(\alpha,\gamma) \cdot G(\alpha,\tau_0) + C(\gamma,g,\tau_0)\}.$$

Since the term in brackets is the reflected intensity, multiplying this by a factor of

$$1 + \Phi$$

will add in the additional contribution to the surface brightness due to the fluorescence. This then modifies the result of equation 36 so that we have

$$q = m_{lim} + D(I_o,\Delta) - H_o - 11.64 + 2.5 \log [\sin^2 \alpha \{\{p(\alpha,\gamma)G(\alpha,\tau_o) + C(\gamma,g,\tau_o)\} (1+\Phi)\}] - \{\frac{\mu_o - |\mu_o|}{2\mu_o}\} \cdot 2.5 \log[\exp(-\tau_o/|\mu_o|)]. \quad (40)$$

Again, one assumes a value for Φ and repeats the computations. The parameter Φ has the same interpretation as it did in the spectrophotometry discussed in the previous section, where it was shown that possibly $.1 \leq \Phi \leq .3$, neglecting the photographic errors.

The calculations were repeated with $\Phi = .1$ and .3. The results are shown as the last two sets of entries in Table III. Note that the assumption of an additional 30% of the reflected light appearing as continuous fluorescence would nearly bring the albedo determined in this way into agreement with the other scattered light results, assuming $g = 1/3$. However, even $\Phi = .3$ is possibly not sufficient to reconcile the difference if $g = .6$.

IV. THE OBSERVATIONAL SEARCH FOR FLUORESCENCE

1. The Photoelectric Technique

The essential idea behind the photoelectric technique employed in the observations to be described here is very similar to the photographic method just discussed. The problem is to determine a measure of the intensity of the continuum and that of the center of an absorption line in both the star and the nebula. Continuous fluorescence will then manifest itself in that the line will appear to be deeper in the star, since here it will not be filled in.

To do this, two pairs of interference filters were used, one member of each pair being considerably wider than the other. Both members of each pair have their peak transmission at the same wavelength. The continuum level can be determined with the wider interference filter and the narrow filter is used to determine the intensity at the line center. The difficulties involved with the non-linearities of the photographic plate at low light intensities have been avoided by using a photoelectric photometer (standard 1P 21 tube). A conventional single channel pulse counting circuit was employed in these observations.

2. Selection Criteria

Since a search for fluorescence is the objective of the observational investigation being discussed here, the reflection nebulae which are to be included in the program should be those in which the preliminary indications of fluorescence are strong and the conditions for the detection of fluorescence are most favorable. In his "Catalog of Bright and Diffuse Nebulae", Cedarblad (1946) lists over two hundred

nebulae. From this list, all nebulae which satisfied the following conditions were considered as possible candidates for inclusion on the observational program:

1) The nebula must be north of -25°. This condition reduces the problem of observing the nebula through large air masses.
2) The illuminating star must be of spectral type A or B. This condition was imposed because the sensitivity of the technique depends on the depth of the absorption line, as discussed by Grainger and Ring (1961).
3) The reflection nebula must be illuminated by only one star. This will simplify comparison of the nebular observations with those of the star.
4) The nebula must be larger than 5' by 5', in order that there is an adequate region of relatively uniform surface brightness.
5) The surrounding region must not be so filled with background stars that it is difficult to find an area free of stars from which to determine the brightness of the night sky.
6) Preference for inclusion is given to those nebulae which overstep the Hubble relation.

In addition, one observational control was included (15 Sextantis). This is a star of spectral type A which is in a region of sky which is free of both nebulosity and background radiation. Data were taken near to the star where scattered starlight could be observed and treated as if it were nebular light. This light was then reduced in the same fashion as the actual observations in order to insure that there is nothing in the technique which gives a false indication of fluorescence.

The two objects which are the most interesting in that they most strongly overstep the Hubble relation were not included in the observations. These two are Barnard's nebulae B 10 and Cedarblad 201. Both of these objects were found to be sufficiently small and faint that the signal to noise ratio considerations made accurate observations prohibitively long .

3. List of Objects Which Were Observed

The nebulae which were observed were NGC 1435, NGC 2068, and IC 1287.

4. The Observations

Two hydrogen lines were selected for the observations, H_β and H_δ (λ = 4861 Å and 4102 Å, respectively). These lines were selected for two reasons: first, they are not near enough to any prominent sky features that sky variations are likely to pose problems of rapid background fluctuation and second, these hydrogen lines are far enough from adjacent hydrogen lines to avoid overlap when the wide band filter is being used. The transmission profile of the H_δ filter pair is shown in Figure XV and was obtained from the calibration curves provided by the manufacturer, Dell Optics, Inc. The H_β filter pair was borrowed from the Kitt Peak National Observatory (their numbers 9 and 494). The hydrogen line H_ζ (λ =3889 Å) would also have been an acceptable line for use in this investigation, but the blocking of shorter wavelengths requires that the filter have such a large physical thickness that it would not fit into a standard filter bolt.

The telescope used in making these observations was the No. 1 - 36" reflecting telescope of the Kitt Peak National Observatory.

This telescope was used in the f/7.5 focus in order that a given diaphragm size should correspond to the largest possible field of view, thus admitting light from as much of the surface of the nebula as possible. This choice of focal ratio, however, does entail a somewhat larger widening of the filter bandpass due to the fact that the edge rays strike the surface of the filter at a somewhat larger angle of incidence than would be the case if the f number were larger. The diaphragms used in these observations were 2.5 and .7 millimeters, corresponding to 75 and 21 " of arc, respectively.

5. Calibration of the System

To see how the amount of fluorescence can be determined quantitatively, we let W and N respectively denote the count rate through the wide and narrow filters and let the subscripts s and n denote the star and nebula. Then we may define the parameter R by

$$R = \left(\frac{N_n}{W_n}\right) \cdot \left(\frac{W_s}{N_s}\right). \tag{41}$$

If there is no fluorescence, the ratio of N to W for both star and nebula should be the same, and R would be equal to unity. However, fluorescence will fill in the nebular (reflected) line and cause R to be greater than unity.

To calibrate this parameter quantitatively, note that if $I(\lambda)$ is the intensity of the star as a function of λ, then

$$N_s \propto \int_0^\infty I(\lambda)\, T_N(\lambda)\, d\lambda \tag{42}$$

and

$$W_S \propto \int_0^\infty I(\lambda)\, T_W(\lambda)\, d\lambda, \qquad (43)$$

where $T(\lambda)$ is the transmission of the filter at wavelength λ. Using photographic spectra of the stars illuminating the various nebulae, the function $I(\lambda)$ was obtained on computer cards. (These spectra were taken by Witt using the Kitt Peak National Observatory 84 inch telescope. No correction for sky was applied due to the relatively short exposure times involved.) The transmission functions are shown in Figure XVI, and these were punched on computer cards. The integrations indicated in equations 42 and 43 were then carried out numerically with integration steps of 1.3 Å.

To determine the effect of fluorescence on R, we will define the parameter Φ to be the intensity of the component of nebular surface brightness due to fluorescence. We will measure Φ in units of the component of nebular intensity due only to reflection. The nebular count rates may now be represented by

$$N_n \propto \int_0^\infty [I(\lambda) + \Phi]\, T_N(\lambda)\, d\lambda \qquad (44)$$

and

$$W_n \propto \int_0^\infty [I(\lambda) + \Phi]\, T_W(\lambda)\, d\lambda. \qquad (45)$$

Various values of Φ were assumed and the integrals of the last four equations were evaluated numerically. Figure XVI shows a graph of R as a function of the value assumed for Φ and computed from these four integrals.

6. The Two and Three Slot Systems

Two other possible systems were considered for the determination of ϕ. Both of these alternatives were essentially monochromators, and both would have employed the dual channel scanner under development at Kitt Peak. In these systems, there were no filters. Instead, the light was to be directed onto a grating and the range of wavelengths which was permitted to fall of the photocathode was determined by the width of one or more exit slots. The wide and narrow filters would thus be replaced by wide and narrow exit slots and the scanning capability of the scanner would not be utilized.

A more sophisticated exit slot, having the configuration shown in Figure XVII was also considered. This would permit the determination of the continuum level without contamination by the line intensity. The intuitive feeling that such an exit slot ought to be more sensitive in detecting fluorescence was checked by repeating the integrals of equations 44 and 45 with the transmission functions of the filters replaced by those for the slots. The slot transmission functions were taken to be as shown in Figure XVIII.

As can be seen from the plots, there are several parameters which can be adjusted. In the two slot system, these are W_c, the width of the central slot and W_w, the width of the wider slot. For the "three slot system", the width of the outer slots, W_o, as well as the displacement from the line center (denoted by D_o), can be adjusted to suit our needs.

In order to determine the most suitable system to be employed for the search for fluorescence, a standard value of 20% fluorescence

was assumed (Φ = .2) and the value of the parameter R defined in equation 41 was computed as a function of the various parameters. The set of parameters which optimizes R was then determined by trial and error. It was found that the general dependence or R is in good agreement with what one would expect intuitively: the system becomes more sensitive with decreasing W_c and more sensitive as the width of the outer slots or the wider slot is increased. Note however that the gain in sensitivity which one buys by reducing the width of the narrow slot will be in practice partially offset by a reduction in count rate due to the fact that less radiation will be permitted to reach the phototube. As a rough compromise, a central slot width of 5 Å was chosen for both the two and three slot systems. (Slot dimensions are given in terms of the wavelength interval which they permit to pass.) The wide slot for the two slot system was chosen to be 180 Å wide. The outer slots of the three slot system were 40 Å wide and had their centers located 37 Å from the line center. The reason that even larger widths for the outer slots were not chosen is that the additional sensitivity which was gained by going to larger slots was rather small and such large slots increase the danger of including a discrete sky feature. There is also the problem of contamination by neighboring hydrogen absorption lines if the system were to be used at H_ζ, which was intended. Figure XIX shows a plot of the value of R as a function of Φ for each of the three transmission functions considered. The three slot system is seen to be the most sensitive and the interference filters are the least sensitive.

Unfortunately, problems of instrumental noise made it impossible to conduct the observations on the three slot system, although the slots were actually constructed and three nights of observations were made on

this system.

The benefits to be derived from conducting the observations on the three slot system are certainly overstated in Figure XIX , although to what extent it is difficult to tell. The essence of the reason for the unreliability of the results shown in Figure XIX is that the transmission functions which were used to derive the R values for the two and three slot systems are not correct. The design of the Kitt Peak spectral scanner is such that the wavelength resolution decreases with increasing diaphragm size. The desire to have as large a diaphragm as possible when observing a faint extended object will result in a rounding of the edges of the transmission curves shown in Figure XVIII. The question of how this will affect the sensitivity of the system was never investigated quantitatively since no observations were used which employed this system.

7. Instrumental Corrections

There are four major corrections to the observational data which are necessary. They are

1) Correction for the intensity due to the night sky.
2) Correction for scattered light from the illuminating star.
3) Corrections for contamination of the star observation by light from the nebula.
4) Corrections for dead time when bright stars are observed.

a) The Night Sky Correction

Since the surface brightness of the night sky is not negligible compared to the observed values of the surface brightness of reflection nebulae, it is imperative to subtract the former from the

latter. In principle, this simply means that one observes the sky in a region free of nebulosity and faint stars for sufficiently long times that it is possible to subtract the sky background from the observations.

In practice, two difficulties arise which make the determination of the correction for sky more difficult than it appears to be at first glance. The first of these difficulties is that the sky background as measured at a fixed point, free of nebulosity and faint stars, will show significant variations over short time periods. The second difficulty is that it is not always easy to decide which region of the sky is "typical", due to the frequently complex structure of regions surrounding many reflection nebulae.

The seriousness of the temporal fluctuations of the sky background depended to a large extent on the particular night which one considers. An example of a bad night (November 10-11, 1971) is shown in Figure XX. These observations were made at a zenith angle of about 30° by counting through the wide filter for 100 seconds at the sky correction point used for NGC 1435. The error bars are determined by dividing the square root of the observed number of counts by 100 seconds. It is readily seen that rapid variations which are not due to photon stastics may be encountered in periods of less than two minutes on a poor night. On good nights, similar plots of sky brightness as a function of time show a sky brightness which does not fluctuate by more than an amount attributable to photon fluctuations for periods of more than an hour.

Therefore, at the beginning of each night of observing, the sky background was monitored to determine the time scale of the fluctuations. An attempt was made to keep the integration times smaller than the typical fluctuation times. In instances in which this was

not possible, the data had to be rejected. The practical considerations of having to move the telescope between nebula and sky made it impractical to consider integration times of shorter than 50 seconds in duration. The star was observed through both the narrow and wide filters at the beginning and end of each observing run and during the course of each run at intervals of approximately every 30 to 45 minutes. After the initial stellar observation, the sky was observed through both filters, then the nebula, then the sky again. Integrations through the wide filter were 50 seconds in duration, while the narrow filter integrations varied in duration from 50 to 450 seconds, depending on the constancy of the sky background. The sky values were then averaged and subtracted from the nebular count rates.

The most difficult aspect of making the sky correction is in deciding where to choose the point which one considers to be "typical sky". In the case of IC 1287, the decision is rather easy, for the edges of the nebula are well defined and there is very little surrounding nebulosity (see Figure XXI). The region selected for the sky correction is marked with an "S". The more difficult nebulae are NGC 1435 and NGC 2068, in which the surrounding region is complex in structure (see Figures XXII to XXIV). In selecting a region which is completely free of nebulosity, one runs the risk of failing to correct for any foreground material, should there be significant contributions to the observed surface brightness from such material. Since it is not known to what extent the material seen surrounding a given nebula is foreground or background, it is necessary to make an assumption on this question and to then attempt to see how changing this assumption alters the results.

Figure XXIII shows the region surrounding NGC 1435 and two regions which were selected as sky correction regions. The region marked S' was chosen on the assumption that it might be typical of the contribution of foreground material. The observations made on this nebula between September 12 and 19, 1971, and between November 9 and 15, 1971, were made using sky position S', while the observations between January 12 and 19, 1972 were made using sky observations taken at position S. Dr. Conard C. Dahn, of the U. S. Naval Observatory, was kind enough to provide me with a discussion of the question of the sky background correction in this region, and it was he who drew my attention to the particularly clear patch of sky near BD +22° 532. When the September data were reduced, it was found that the values of R which were obtained were consistently smaller than unity. It is very difficult to imagine a physical mechanism which could give rise to such an effect, for it would indicate that the lines in the reflected spectrum are deeper than they are in the spectrum of the illuminating star. The possibility that illumination by the GSF might produce such an effect was considered, but as will be shown later, a calculated value for R for the GSF indicates that such illumination should in fact have the effect of raising R above unity.

Note however that if one were to subtract too much sky background from the nebular observations, this would have the effect of reducing R from the true value, since the sky background is essentially continuous. Only when the observations were reduced using the sky corrections as determined from observations obtained at position S were the R values raised to unity. During the January observing period, the sky brightnesses at S and S' were compared and it was found that

$$\left(\frac{S}{S_T}\right)_{wide} = .825; \qquad \left(\frac{S}{S_T}\right)_{narrow} = .862 \ .$$

The sky observations of September and November were then reduced by the appropriate constant and the data was reanalyzed. The detailed discussion of the results is postponed until a later section.

The problem of selecting a sky correction point for NGC 2068 has a much less involved history. The initial hypothesis which was adopted was that the dark lane which passes quite near to the sky is a foreground dust lane and that sky observations conducted here should give a firm lower limit to the amount of sky to be subtracted from the nebular observations. Since this entire region is filled with faint nebulosity (much of which is probably hydrogen emission) the selection of the sky point is difficult. However, when the first observations were reduced, it became apparent that the R values which were being obtained were again smaller than unity and the only result which could be expected by changing the sky observation point would be to further reduce R. Hence, all observations were made at this point.

b) The Scattered Light Correction

The second major correction which must be applied to the observations is a correction for light from the illuminating star which is scattered into the photometer. The literature regarding the correction for scattered light is not extensive and the observers who do discuss it do not often do so in detail. The most thorough discussion of this effect seems to be that by Elvius and Hall (1966), who examined the dependence of scattered light as a function of offset distance from a bright star in a region free of nebulosity. They report dependence of the quantity

of such scattered light on wavelength, night, and condition of the optics. Racine (1971), in discussing his photoelectric photometry of the reflection nebula Cedarblad 201, mentions that he avoids making observations in position angles which correspond to directions of the secondary mirror supports in order to avoid interference effects. Since the scattered light intensity may be correlated with so many variables, a systematic investigation was made of this effect by measuring the intensity of the scattered light as a function of offset for the star λ Ursae Majoris during the January observing run.

The scattered light runs were made by observing the star first, then a selected sky region about 25' from the star. Then the scattered light was measured at ever increasing offsets from the star, beginning near to the star and moving outward until the initial sky position was reached again. Then the star was measured again. All scattered light checks were conducted through the wide filter to save time. To prevent the possibility of introducing some systematic effects by always determining the scattered light by increasing the offset, some runs were made in the opposite direction and some were made by skipping around from one offset to another. No significant difference could be found when the results of these different procedures were compared. Due to the narrow bandpass of the H_δ filter with which most of the runs were made, a scattered light run typically required 40 to 50 minutes to make.

The procedure used for reducing the scattered light observations was to average the two star readings as well as to average the sky readings. The sky readings (which also include the dark current) were then subtracted from each of the scattered light readings and this result was normalized to the count rate for the star.

The surprising result of the investigation of the scattered light correction is that it appears to be independent of all of the parameters which were considered. Figure XXV shows data for the scattered light correction for various nights. Inspection of these curves shows that the scattered light correction does not change appreciably from one night to the next, even when a period of several months is involved. Three of the sets of data were taken through the H_δ filter in the North-South direction, so as to lie along a direction in which the diffraction spike due to a secondary support should lie. Another run is along the same direction, but through the H_β filter. It can be seen that there is no appreciable difference in scattering correction between these two wavelengths. Another set of data is shown for the H_δ filter with the run having been made at an angle of 45° with respect to the direction of the secondary supports on the No. 1-36" Kitt Peak reflector. Again we see that the difference between the adopted curve and this set of scattered light observations is slight. The three H_δ runs were all made on different nights, indicating that the scattering does not change with time. Runs for the scattered light correction were made on α Andromedae at two different hour angles in order to determine the effect of air mass on scattered light. On the night of September 14-15, 1971, a scattered light run was made starting at H.A. = $4^{08}\!\!-\!\!E$. and ending at $3^{03}\!\!-\!\!E$., and on September 15-16, 1971 the run was repeated for hour angle starting at $0^{45}\!\!-\!\!E$. and ending at $0^{04}\!\!-\!\!W$. These runs produced nearly identical scattered light correction curves, suggesting that the scattering is occuring primarily in the instrument. Observers planning future work in photometry near bright objects should bear in mind the fact that the light scattering correction must be carefully determined for each individual

instrument. The sensitivity of scattering corrections to seeing conditions reported by some observers suggests that the diaphragm size may be a parameter on which the scattered light depends.

In practice, the scattered light correction for any nebular observation was made by multiplying the normalized correction factor (read from Figure XXV) by the average of the count rates determined for the illuminating star before and after the nebular observation. Attempts to fit the scattered light observations to various assumed functional forms met with little success.

c) The Finite Diaphragm Correction

The third correction which must be considered is the possibility of contamination of the stellar photometry due to inclusion of nebular light in the diaphragm. Note that if fluorescence is present this will result in an underestimate of the fluorescence because the stellar lines will appear to be filled in by the addition of some additional continuous fluorescence in the stellar observations.

In order to investigate this effect, a series of runs was made in which the illuminating star was held fixed in the field of view while the size of the diaphragm was changed. The object selected for this investigation was NGC 2068 because it is a bright nebula illuminated by a faint star. If we let ρ be the observed count rate, S be the stellar contribution to the count rate, A be the diaphragm area, and B be the surface brightness of the nebula in units of count rate/area,

$$S = \rho - BA, \tag{46}$$

assuming a uniform surface brightness. The form of equation 46 indicates that the true stellar count rate could be determined by plotting

observed count rate as a function of area of the diaphragm and extrapolating the resulting linear function to zero diaphragm area. There is a systematic error which could be introduced into this determination. The diaphragm may begin to cut off some of the star image as we move to smaller areas, causing S to decrease more rapidly than as a linear function of A.

Figure XXVI shows the results of several of these runs. Note than there is no indication of a significant downward curvature of the curve at the smaller areas. The uncertainties due to statistical fluctuation are shown as error bars or else are the size of the dots. The point for A = 1.33 mm^2 is seen to lie systematically too high for the linear curve. A possibility which immediately suggests itself is that the diaphragms are not machined with sufficient accuracy to guarantee the reliability of this approach.

To determine whether or not the non-linearity of the curves in Figure XXVI might be due to machining inaccuracies, note that differentiation of equation 46 gives

$$\delta\rho = B\ \delta A = B(\pi d \cdot \delta d), \qquad (47)$$

where d is the diameter of the diaphragm. As an example, consider the results for the narrow H_β filter. The linear fit is 30 counts/second too low, compared to the observed count rate at A = 1.33 mm^2. Inspection of the curve at A = 1.00 mm^2 gives B = 550 counts/second/mm^2; substituting these numbers into equation 47 shows that δd, the inaccuracy of the diaphragm diameter necessary to explain the observed deviation from the curve, is about .004 mm or about .0002 inch. Thus, for machined diaphragms of the type employed for this investigation, this difference

can easily be due to machining tolerences. A more accurate investigation would reguire the use of etched foil diaphragms.

The stellar count rates for NGC 2068 were corrected by extrapolating the curves of the type shown in Figure XXVI to zero diaphragm. However, the correction was found to be negligible for all of the other nebulae investigated because they were illuminated by brighter stars and had lower surface brightnesses.

The final correction which was applied to the data was a correction for dead time which was necessary for the brighter stars. If ρ is the observed count rate, the true count rate, ρ_o, is

$$\rho_o = \rho \left(1 + \frac{\rho}{20 \times 10^6}\right) . \qquad (48)$$

This is the standard formula used for correction for dead time, the value of 20×10^6 having been provided by Jeannette Barnes of the Kitt Peak staff.

8. The Problem of Noise

Physically, there are at least three sources of noise which are to be expected in the observations. They are

1) Fluctuations in the number of signal (nebular) photons arriving,
2) Fluctuations in the number of background (sky) photons arriving,
3) and dark current counts.

The observations have been conducted for sufficiently long that the number of counts involved is large enough that the statistical uncertainties are given by the square root of the number of counts. It is then a straightforward matter to derive an expression for the ratio of signal to noise as a function of the integration time, t. If we let

C_s be the number of signal photons arriving at the photocathode/unit time, the total number of signal counts, S, is

$$S = 1/2\ QC_s t,$$

where Q is the quantum efficiency of the tube and the factor of 1/2 arises because half of the observing time is devoted to monitoring the sky background. The uncertainty due to the fluctuation in the dark current background, and signal counts will give rise to a noise, N, of

$$N = \sqrt{(C_d + 1/2\ QC_s + QC_b)t}\ ,$$

where C_d and C_b are the dark and background rates for a photomultiplier. (Note that C_b is sky plus scattered light intensity.) Thus the signal to noise ratio is

$$\frac{S}{N} = \frac{1/2\ QC_s t}{\sqrt{(C_d + 1/2\ QC_s + QC_b)t}}\ . \qquad (49)$$

Note that the fractional uncertainty in the data is $(S/N)^{-1}$. In order to see the typical values involved in observations through the narrow band filter, an estimate of the uncertainty in the observations of NGC 1435 follows. Taking C_d as 2 counts/second, QC_b as 36 counts/second, and QC_s as 24 counts/second, an integration time of 1600 seconds gives 1% accuracy in the case that the system is limited by photon noise. It will be seen later that this was not the case and that the accuracy which was obtained was actually not this high.

It was hoped that the three slot system would prove superior (in the sense of a higher signal to noise ratio) than the interference filter system. However, the instrumental losses in the scanner were

considerably higher than expected so that the actual count rate through the scanner was reduced by nearly a factor of two. The photomultiplier had a dark count rate of 10 counts/second, about five times as high as the interference filter system. Consequently no successful observations could be made using this system.

9. The Data Reduction Technique

Most of the corrections which were applied to the data have already been discussed. The primary purpose of this section is to summarize these corrections, indicating the order in which the corrections were applied. Certain details not previously discussed are also included here.

All observations were recorded twice, once in an observing notebook and also by an automatic printer. Integration time, filter bolt position, sidereal time, and total count were recorded. These numbers were then punched on computer cards and the remainder of the data processing was done automatically, employing a program named PERED.

Each card contained information identifying it as to whether it was an observation of a star, sky, or nebula. The ratio of narrow to wide count rate for the stellar observations was computed immediately after the correction for dead time was applied to the stellar observations. No correction for dead time was applied to the nebular data, since the correction was negligible for such faint objects. The sky readings before and after the nebular observation were averaged to correct for temporal variations to first order. (For the observations of NGC 1435, sky observations made in 1971 were corrected to the 1972 values using equations discussed in Section IV - 7.) These sky intensi-

ties, which also contain the dark current, were then subtracted from the nebular intensity. Next, the star count rate was multiplied by the scattered light correction appropriate to the particular offset distance involved and subtracted from the nebular count rate. This process was carried out for both the wide and narrow filter observations.

The ratio of narrow to wide count rate, R_*, which was adopted for the data reduction was the average of all individual R_* values. For the nebular observations, the averaging was postponed. For each nebular observation, the value of R defined in equation 41 was computed and stored in the computer. Then the average and rms deviation for the set of nebular observations was computed. Any values of R which deviated from the mean by more than 3 standard deviations were deleted from the data deck and the calculations were repeated. The results of this second calculation were again examined and any data leading to a value of R which deviates from the mean by more than two standard deviations were removed and the calculations were repeated with the resulting data deck. The adopted value of R was obtained by averaging the R values obtained from this last run.

The observations of the control star, 15 Sextantis, were reduced in the same manner except that no scattered light correction was applied. As a check on the accuracy of the scattered light correction technique, the control observations were also reduced, including this correction. When this was done, the "nebular" intensity results were found to be distributed uniformly about zero.

10. The Observational Results

The results of the observations and data reductions which have been described are displayed in Table IV. The first column lists the nebula, the second gives the wavelength, the third lists the position number and the fourth and fifth columns indicate the north-south and east-west offsets of the point observed in minutes of arc measured from the illuminating star. The "R" column is the value of R determined by the method just discussed and σ is the rms deviation of the individual observations from the quoted result. The "t" column is the total number of seconds of narrow band filter time which were included in the determination of R. Thus, the time spent on determining the sky background is not included in this number. The observing time spent on making observations which were ultimately rejected is also omitted from this number.

V. THE IMPLICATIONS OF THE OBSERVATIONAL RESULTS

Inspection of the results presented in Table IV immediately indicates that there is no evidence for fluorescence to the accuracy with which it can be detected by this technique. All of the values determined for R appear to be within about one standard deviation of unity except for the NGC 2068 results which are systematically too low.

1. The NGC 2068 Results

Several possibilities for the low values of R as determined for NGC 2068 were considered. Since the star is quite faint and the surface brightness of the nebula is high, the effect of the nebular light admitted through the finite diaphragm was taken into account by applying the finite diaphragm correction discussed in Section IV, part 7. It was found however, that the change which resulted in the value of R was negligible.

The low values of R are probably due to the presence of a faint star which was included in the diaphragm during the observations. This star is about 1.5 magnitudes fainter than the illuminating star of NGC 2068 and is located about 5" east of the illuminating star. This star could easily alter the value of the narrow to wide count rate ratio for the stellar observations, giving rise to the observed discrepancy.

2. The Possibility of Small "Strömgren Spheres"

Consideration was given to the possibility that the narrow to wide count rate ratios obtained for the stellar observations might

be affected by the presence of small Strömgren spheres. Although such HII regions would be unobservable as an extended object, the possibility was investigated that the normal amount of interstellar hydrogen present near a star might give rise to hydrogen emission lines which would contaminate the stellar results.

In order to estimate the magnitude of this effect, one may follow Spitzer (1968) and define the emission measure as

$$E_m = n_e^2 \, L \text{ pc/cm}^6 \quad ,$$

where n_e is the number of electrons/cm^3 and L is the thickness of the emission region in the line of sight, measured in parsecs. In order to convert the emission measure into the number of counts/second on the instrument with which the observations were conducted, we may note that Johnson (1968) gives a theoretical expression for the volume emissivity of an HII region as

$$\varepsilon(H\alpha) = 2.6 \times 10^{-26} n_e^2 \quad .$$

Here, ε is the power emitted in Hα in ergs/cm^3/sec/ steradian and n_e is the electron density. Assuming that the power emitted in Hδ is the same, one finds that a density of approximately 60 electrons/cm^3 will produce a small Strömgrem sphere which is just at the limit of detection with this technique. Since this hydrogen density is far higher than it is reasonable to expect, such HII regions may be excluded as a possible reason for the failure to detect fluorescence.

3. Fluorescence and Particle Models

Table IV shows that for the best determined case, that of NGC 1435, R=1.00±.02 is a reasonable summary of the results. Consulting Figure XVI, we see that an rms deviation of .02 in the value of R

corresponds to an rms deviation of about 10% in the value of Φ. Thus, if any continuous fluorescence is present, it accounts for less than 10% of the total surface brightness in a reflection nebula. The fact that little or no continuous fluorescence is observed in reflection nebulae can serve to eliminate from further consideration any particle model which would predict such fluorescence. This criterion, however, constitutes a rather insensitive test when it is applied to discriminate between particle models.

A study of fluorescence bibliography of Passwater (1967) indicates that few of the materials which have been considered as possible constitutents of the interstellar medium fluoresce when irradiated by x-rays and that the intensity and spectral distribution of the fluorescence can be altered by the addition of impurities. However, even at -183°C, the quantum efficiency is only of the order of 10^{-4} or less. The mineral enstatite, which has recently been proposed as a possible constitutent of the interstellar medium, is not listed as a fluorescent mineral in the extensive tables of Gleason (1960). As has been previously discussed, enstatite does fluoresce under proton bombardment, but Blair and Edgington (1968) find its quantum efficiency to be only 10^{-3}. Thus considerable amounts of energy in the form of proton flux from the illuminating star would be required to generate an observable fluorescent intensity.

Hence we must conclude that the absence of fluorescence cannot provide any discrimination among the various particle models currently under consideration.

4. Concluding Remarks

Some perspective as to the implications of this investigation can be gained if we briefly retrace the steps which have been taken to this point.

The principal starting point for this work was the Hubble relation between the angular extent of reflection nebulae and the apparent magnitudes of their illuminating stars. Results concerning albedo and phase function of scattering particles as implied by the excellent fit of Hubble's relation with observations of reflection nebulae appeared to be in fundamental disagreement with corresponding results derived from studies of the diffuse galactic light and dark nebulae.

In order to study the source of this disagreement a generalized version of the Hubble relation was derived, which incorporated a forward scattering phase function, arbitrary albedo less than unity and finite optical thickness of the reflection nebula. The surface brightness predicted for nebulae under these conditions is indeed less than that predicted based on the original assumptions of Hubble. The effect of illumination of the nebula by the general interstellar radiation field was found to be inadequate to remove the difference. Fluorescence by the solid particles in the nebula was considered as a possibility to produce the necessary surface brightness. The results of an observational search for such fluorescence indicated in the best studied case that no fluorescence is present in the spectral region under investigation, with a possible rms deviation not greater than 10%. Model calculations as summarized in Table III, however, indicated that at least 30% of the surface brightness of reflection nebulae had to be due to fluorescence if we wanted to invoke the same parameters for albedo and phase function as found from other scattered light studies. Thus we are forced to draw the following conclusions regarding the surface brightness of reflection nebulae:

1. The fluorescence mechanism invoked by Struve and Swings (1948) to explain the extraordinarily large size of B10 and the remark of Aller (1956) that "Some nebulae are actually brighter than the theoretical relation predicts" and that in some instances "...it appears to arise from actual fluorescence in the solid grains" do not appear to be valid explanations of the discrepancies under consideration. The magnitude of the fluorescent contribution to nebular surface brightness required to explain these discrepancies would have been so large that it would have been detected with the observational technique employed here.

2. The calculations which have been presented here, when combined with the observational evidence that continuous fluorescence does not occur, suggest that the albedo of particles in reflection nebulae may very well be higher than the albedo of interstellar particles in general. Further investigations as to possible causes of this difference may prove fruitful for better understanding of reflection nebulae and interstellar particles. It would be of great interest to determine whether the difference in albedo is due to modification of typical interstellar particles or to separation of such particles by size and/or type.

REFERENCES

1. A'Hearn, M.F., 1971, A.J., 76, 264.
2. Aller, L.H., 1956, Gaseous Nebulae, John Wiley & Sons, Inc.
3. Ambartsumian, V.A., and Gordeladse, S.G., 1938, Bull. Ambastumani, 2, 37.
4. Becker, R.S., 1969, Theory and Interpretation of Fluorescence and Phosphorescence, Wiley Interscience.
5. Blair, I.M., and Edgington, J.A., 1968, Nature, 217, 157.
6. Carlstedt, J.L., and Mullikin, T.W., 1966, Ap. J. Suppl. Ser., 12, 449.
7. Cedarblad, S., 1946, Lund. Obs. Medd., Ser. II, No. 119.
8. Chandrasekhar, S., 1950, Radiative Transfer, Dover Publications.
9. Dahn, C.C., Private Communication.
10. Derham, C.J., and Geake, J.E., 1964, Nature, 201, 62.
11. Dorschner, J., and Gürtler, J., 1966, A.N., 289, 57.
12. Elsässer, H., and Haug, U., 1960 Z. Astrophys., 50, 121.
13. Elvius, A., and Hall, J.S., 1966, Lowell Obs. Bull., 6, 257.
14. Gleason, S., 1960, Ultraviolet Guide to Minerals, van Nostrand.
15. Grainger, J.F., and Ring, J., 1961, Physics and Astronomy of the Moon, ed. by Z. Kopal, Academic Press, New York.
16. Greenberg, J.M., 1968, Stars and Stellar Systems, Volume 7, University of Chicago Press.
17. Greenberg, J.M., and Hanner, M.S., 1970, Ap. J., 161, 947.
18. Greenberg, J.M., and Roark, T.P., 1967, Ap. J., 147, 917.
19. Grossweiner, L.I., and Matheson, M.S., 1954, J. Chem. Phys.,Vol. 22, 1514.
20. Henyey, L.G., and Greenstein, J.L., 1938, Ap. J., 88, 580.
21. Henyey, L.G., and Greenstein, J.L., 1939, Ap. J., 89, 647.

22. Henyey, L.G., and Greenstein, J.L., 1941, Ap. J., 93, 70.

23. Hiltner, W.A., 1956, Vistas in Astronomy, ed. A. Beer, 2, 1088, Pergamon Press.

24. Hubble, E., 1922, Ap. J., 56, 416.

25. Hulst, H.C., van de, and de Jong, T., 1969, Physica, 41, 151.

26. Johnson, J.L., 1968, Stars and Stellar Systems, Volume 7, University of Chicago Press.

27. Krishna Swamy, K.D., and O'Dell, C.R., 1967, Ap. J., 147, 937.

28. Lillie, C.F., and Witt, A.N., 1969, Ap. J. Lett., 3, 201.

29. Link, F., 1961, in Physics and Astronomy of the Moon, ed. by A. Kopal, Academic Press, New York.

30. Lynds, B.T., 1965, P.A.S.P., 77, 134.

31. Mattila, K., 1970 a, Astron. & Astrophys., 8, 273.

32. Mattila, K., 1970 b, Astron. & Astrophys., 9, 53.

33. Mattila, K., 1971, Astron. & Astrophys., 15, 292.

34. Merrill, P.W., 1936, Ap. J., 83, 126.

35. Munch, G., 1952, Ap. J., 116, 575.

36. Passwater, R.A., 1967, Guide to Fluorescence Literature, Plenum Press Data Division.

37. Plass, G.M., 1966, Applied Optics, 5, 279.

38. Racine, R., 1968, A.J., 73, 233.

39. Racine, R., 1971, A. J., 76, 321.

40. Roach, F.E., and Megill, L.R., 1961, Ap. J., 133, 228.

41. Slipher, V.M., 1918, P.A.S.P., 30, 63; and 1919, 31, 212.

42. Sobouti, Y., 1963, Ap. J. Supp. Ser., 7, 411.

43. Spitzer, L., 1968, Diffuse Matter in Space, Interscience Publishers, New York.

44. Struve, O., and Swings, P., 1948, P.A.S.P., 60, 61.

45. Walker, G.A.H., Hutchings, J.B., and Younger, P.F., 1969, A.J., 74, 1061.

46. Wampler, E.J., 1963, Ap. J., 137, 1071.

47. Witt, A. N., 1968, Ap. J., 152, 59.

48. Witt. A.N., and Lillie, C.F., 1972, Astron. & Astrophys., to be published.

49. Witt, A.N., and Rush, W.F., 1971, B.A.A.S. (abstract), 3, 389.

50. York, D.G., 1971, Ap. J., 166, 65.

51. Zanstra, H., 1927, Ap. J., 65, 50.

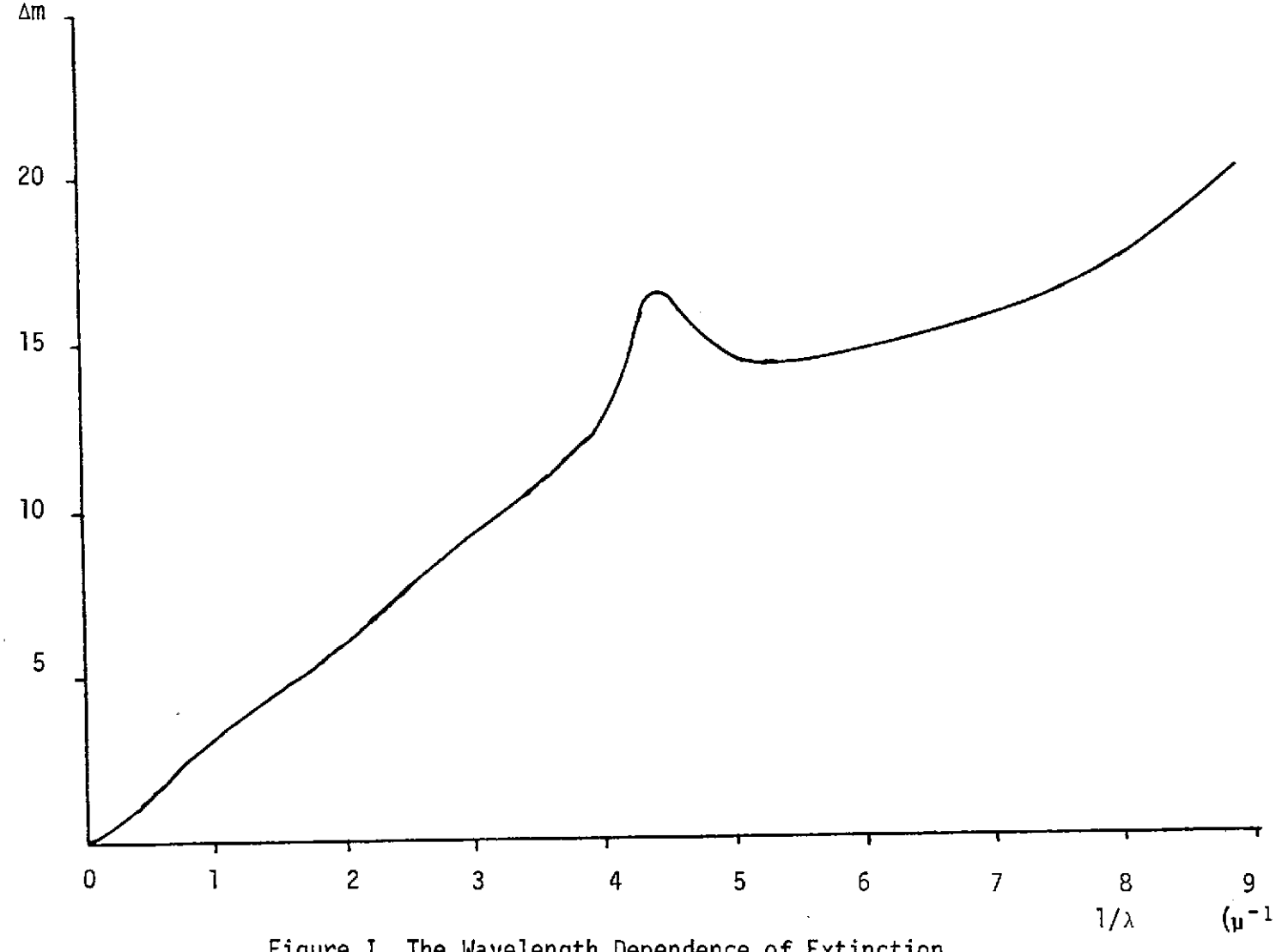

Figure I The Wavelength Dependence of Extinction

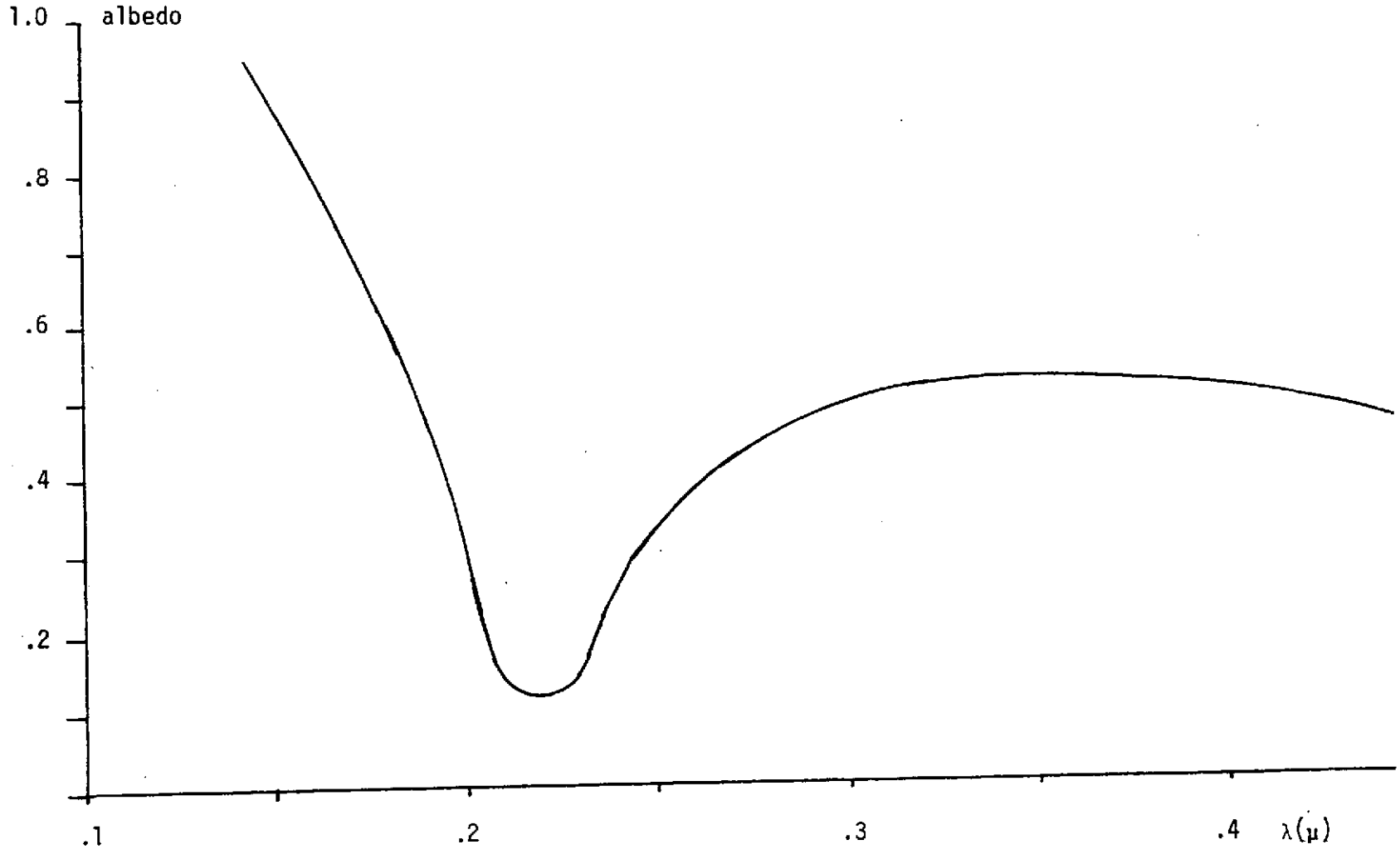

Figure II The Wavelength Dependence of the Albedo of Interstellar Particles

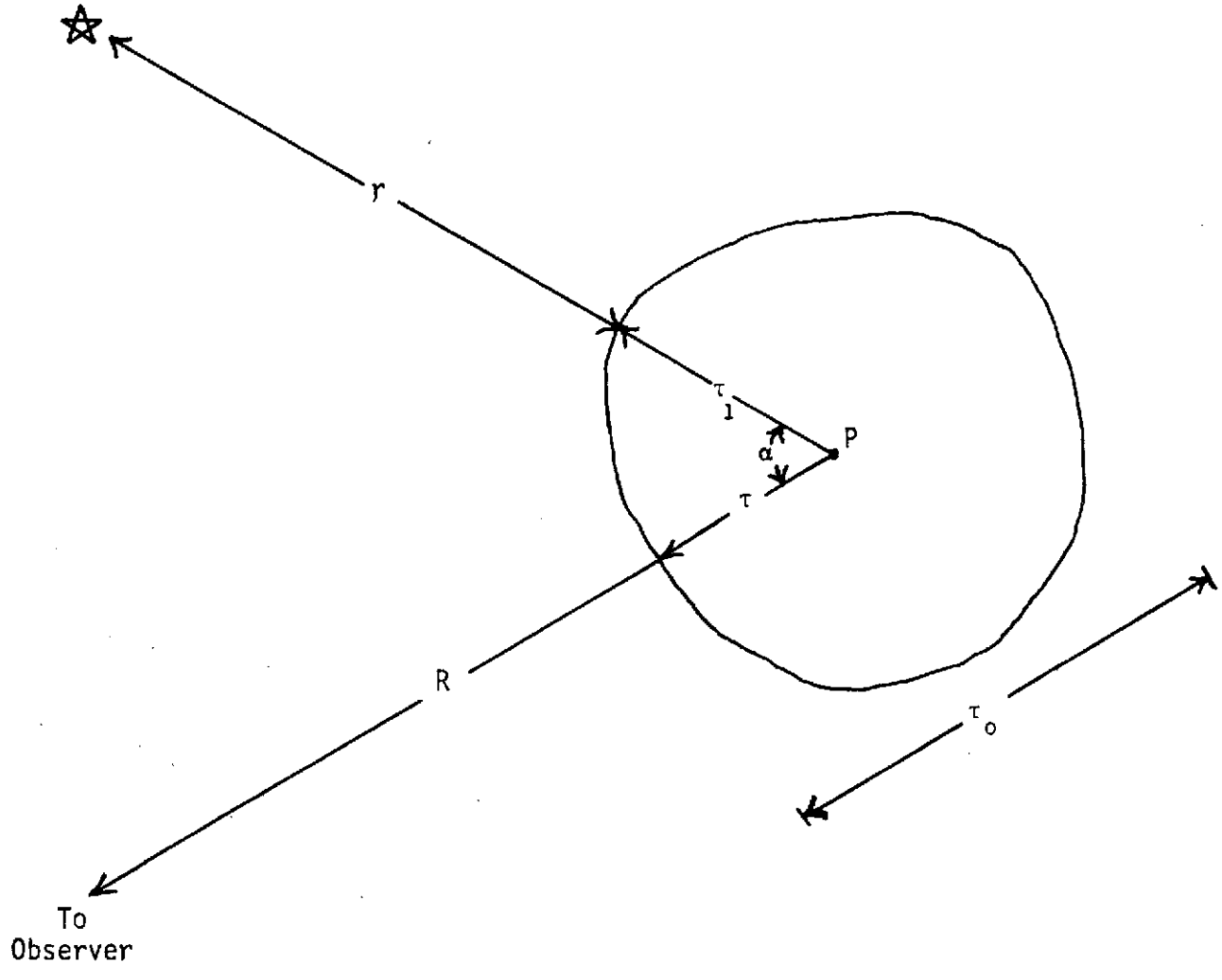

Figure III Geometry Used in Deriving Hubble's Relation

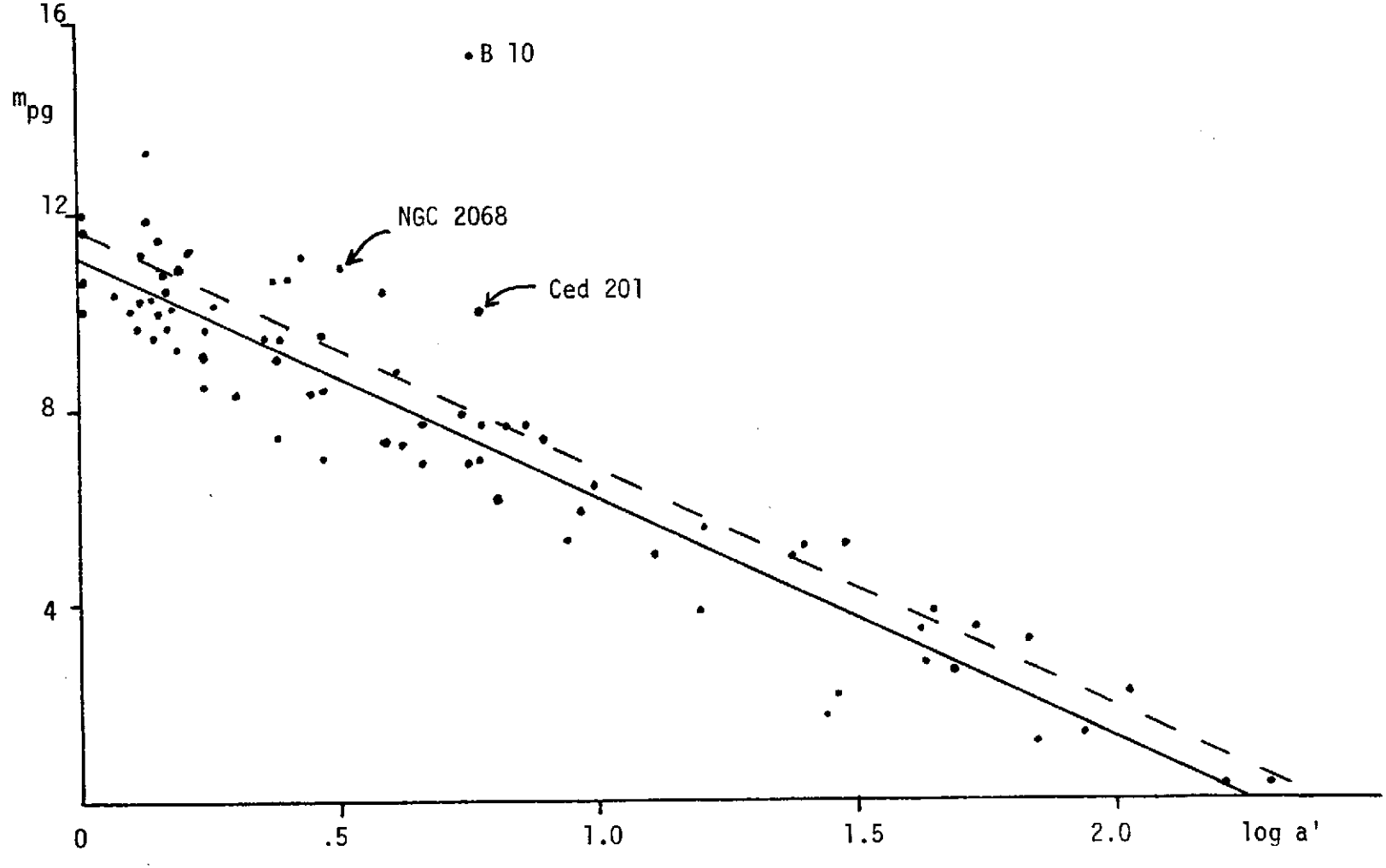

Figure IV Hubble Relation for Reflection Nebulae

The solid curve is a least squares fit to the data and the broken curve is the limiting relation, equation 7.

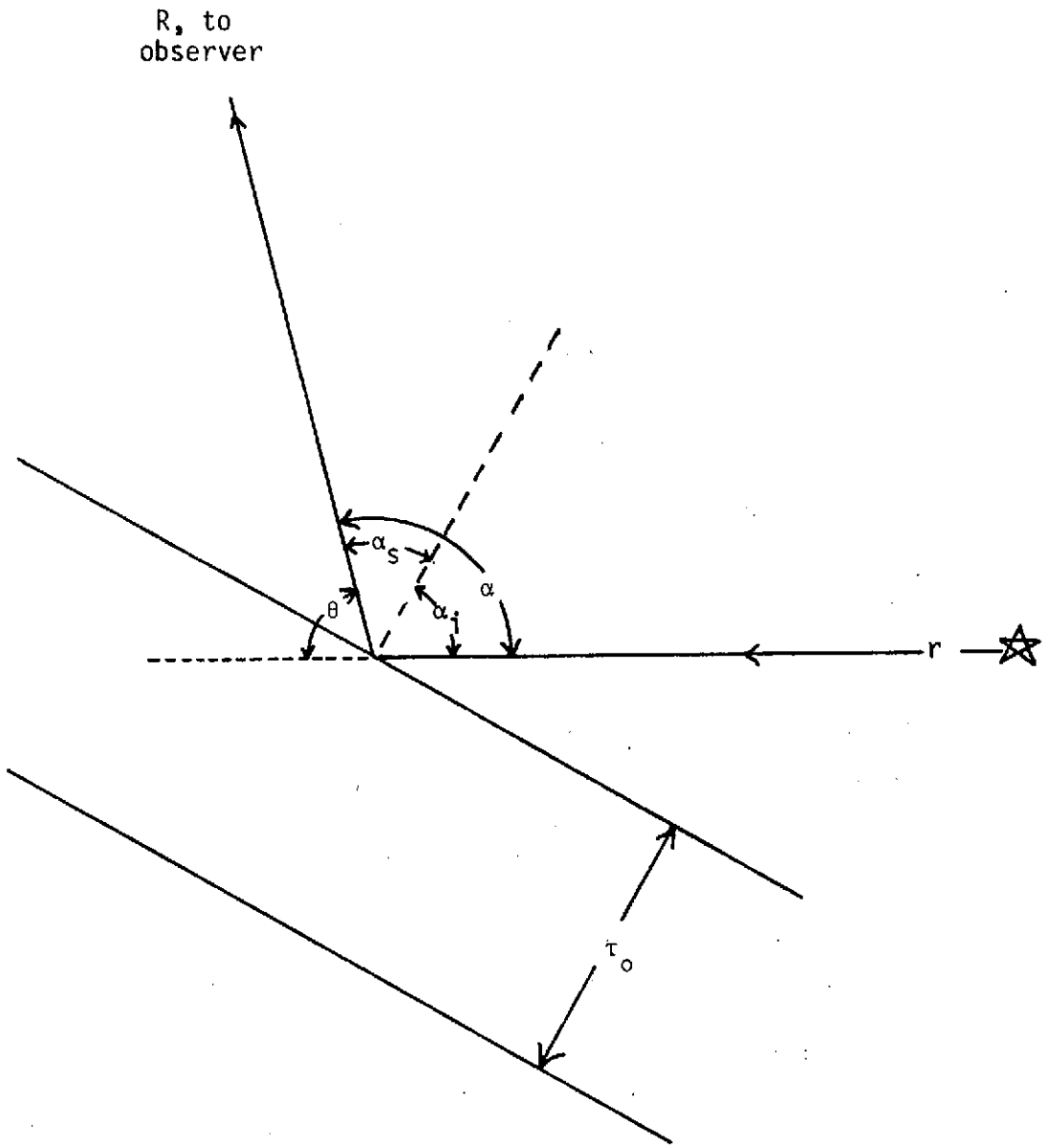

Figure V Symbols Used in the Derivation of the Generalized Hubble Relation

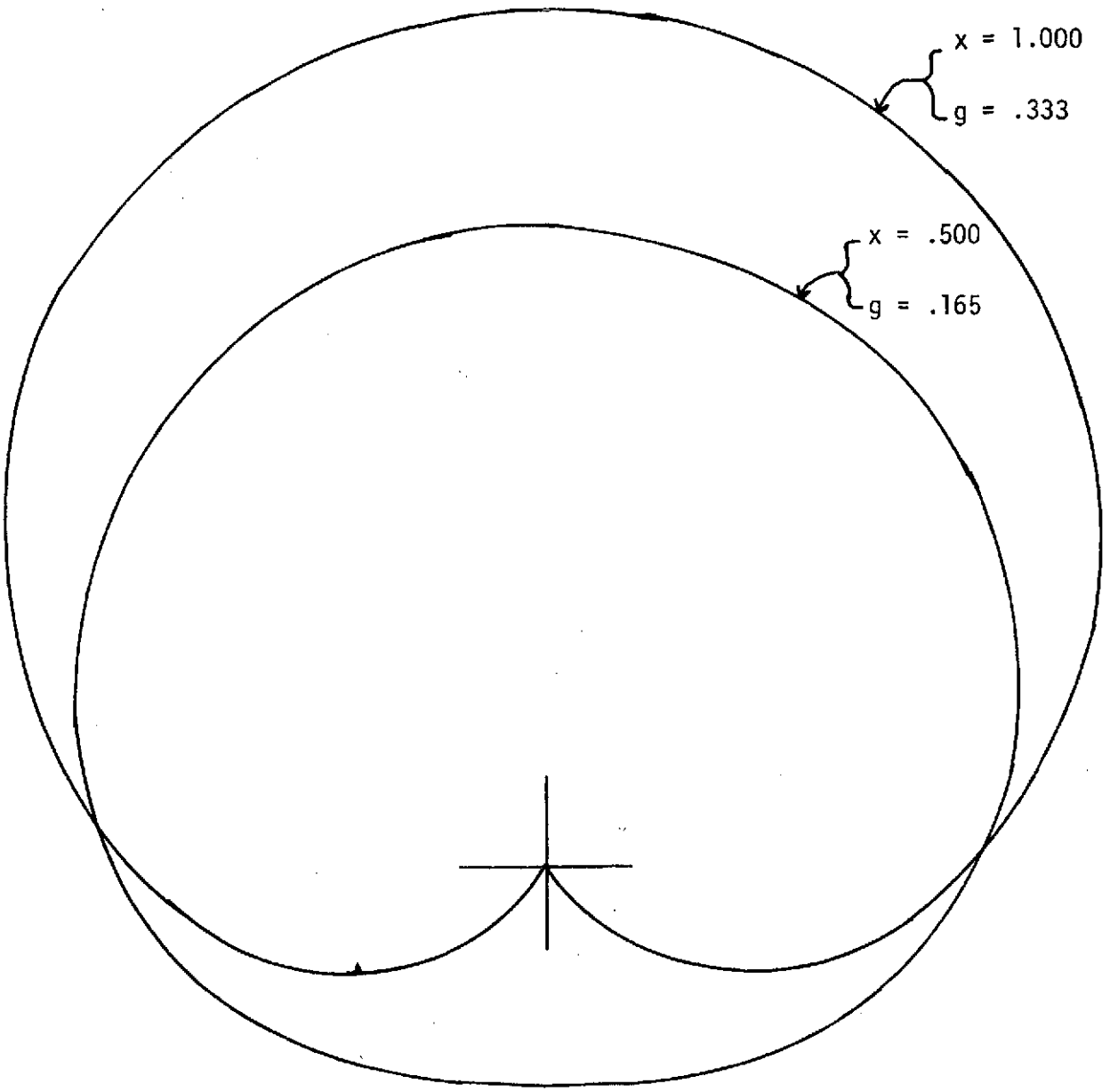

Figure VI The Phase Function of Equation 23 for x = .5 and x = 1

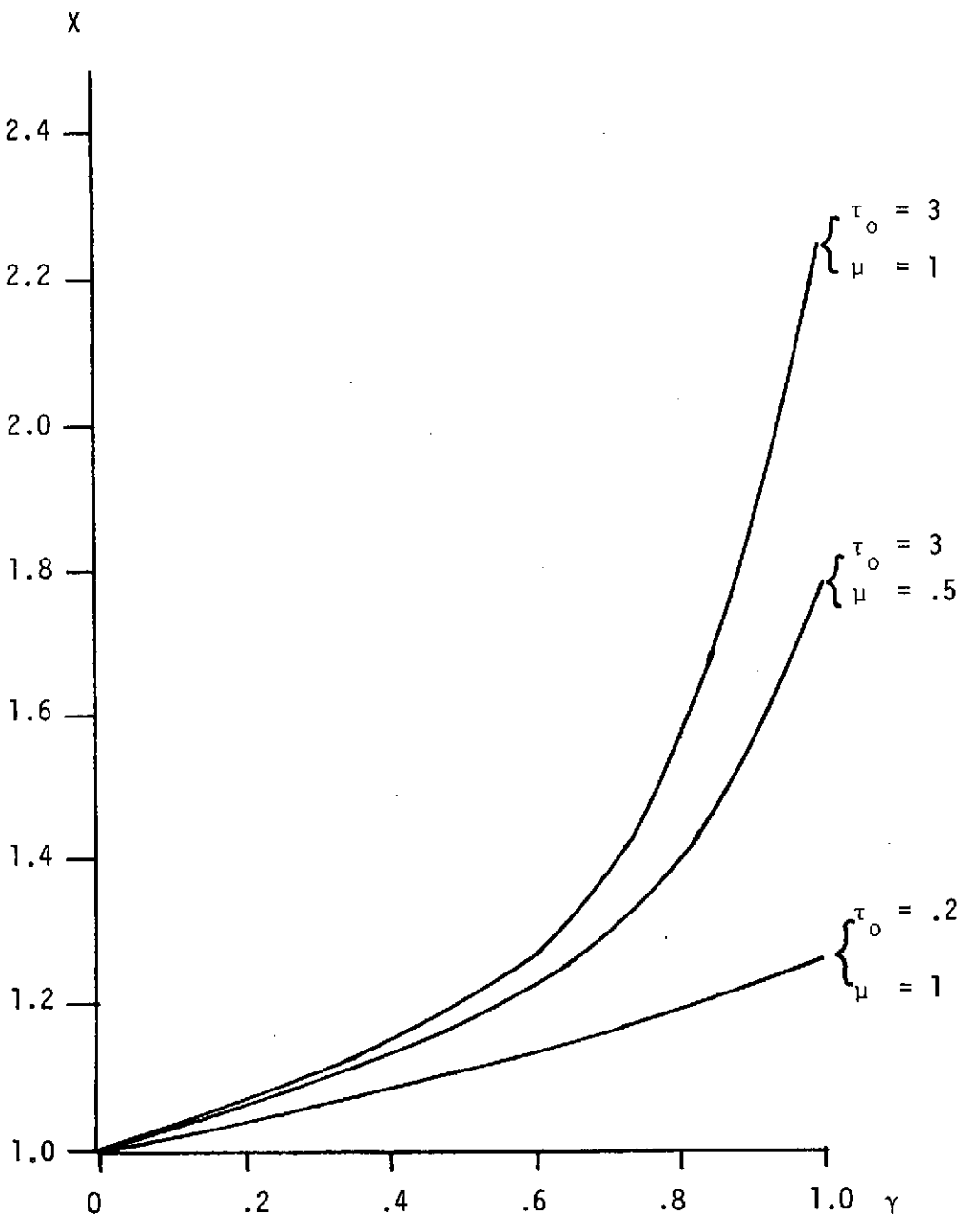

Figure VII The γ Dependence of X for μ and τ_o Values Indicated on the Plot

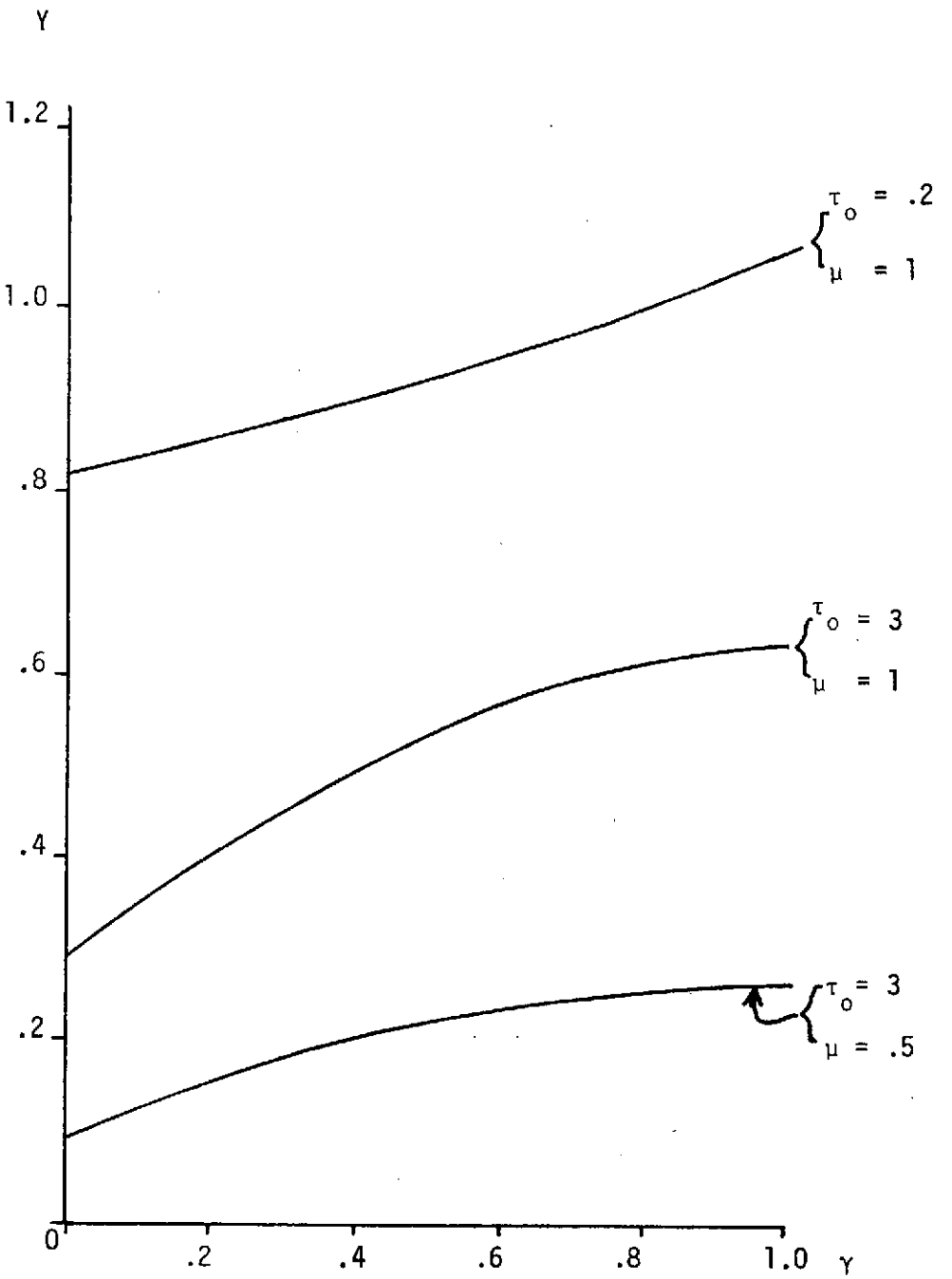

Figure VIII The γ Dependence of Y for μ and τ_o Values Indicated on the Plot

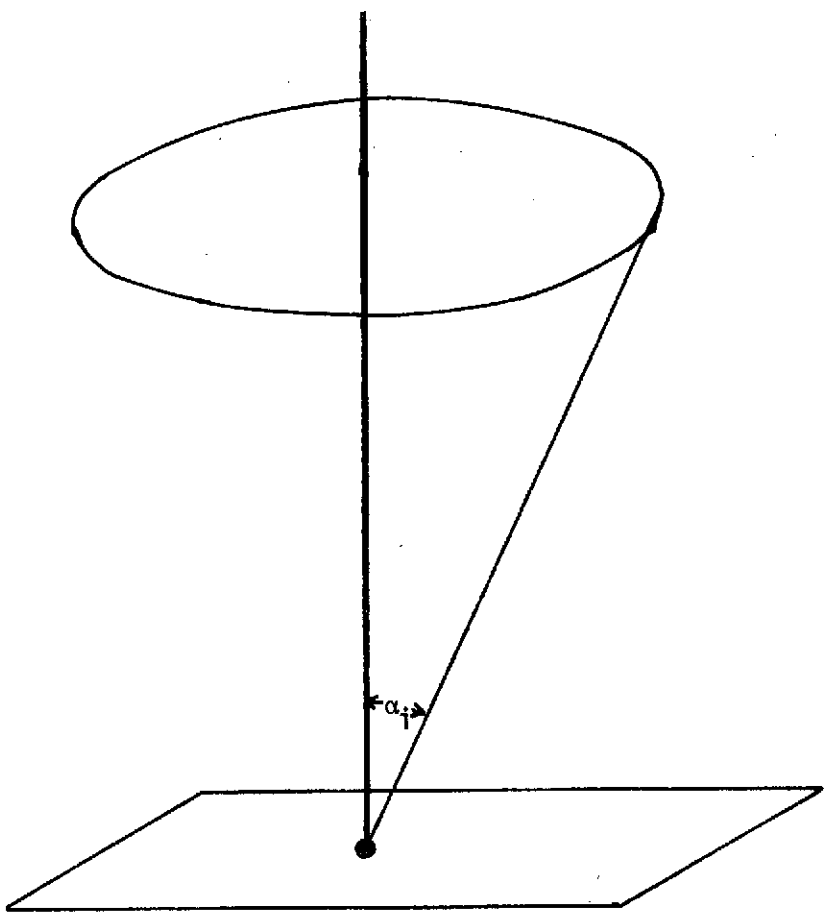

Figure IX The Geometry of the Illumination of the Nebula By a Uniform Hemisphere

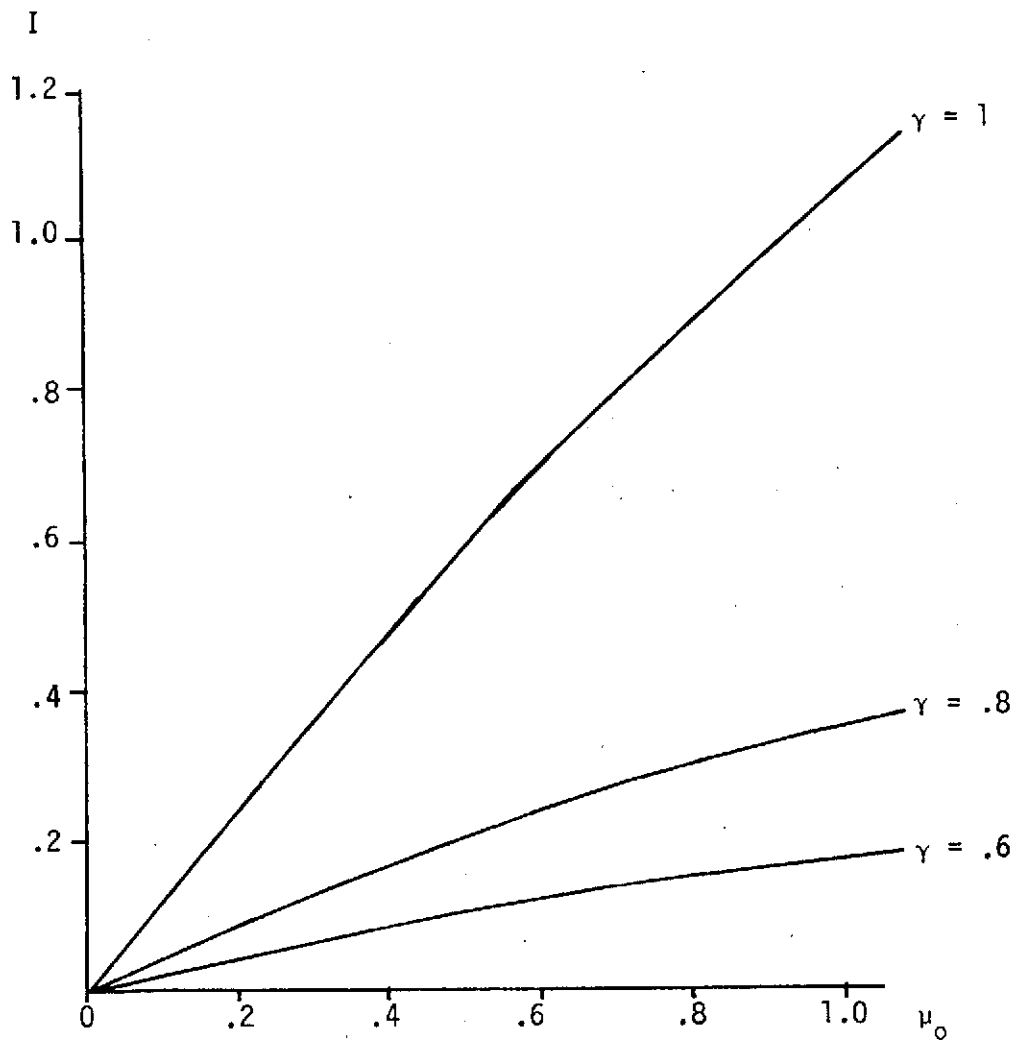

Figure X Reflected Surface Brightness for g = 0, μ = 1, $\tau_o = \infty$ As a Function of μ_o. Surface Brightness is in Units of I_o, The Incident Intensity.

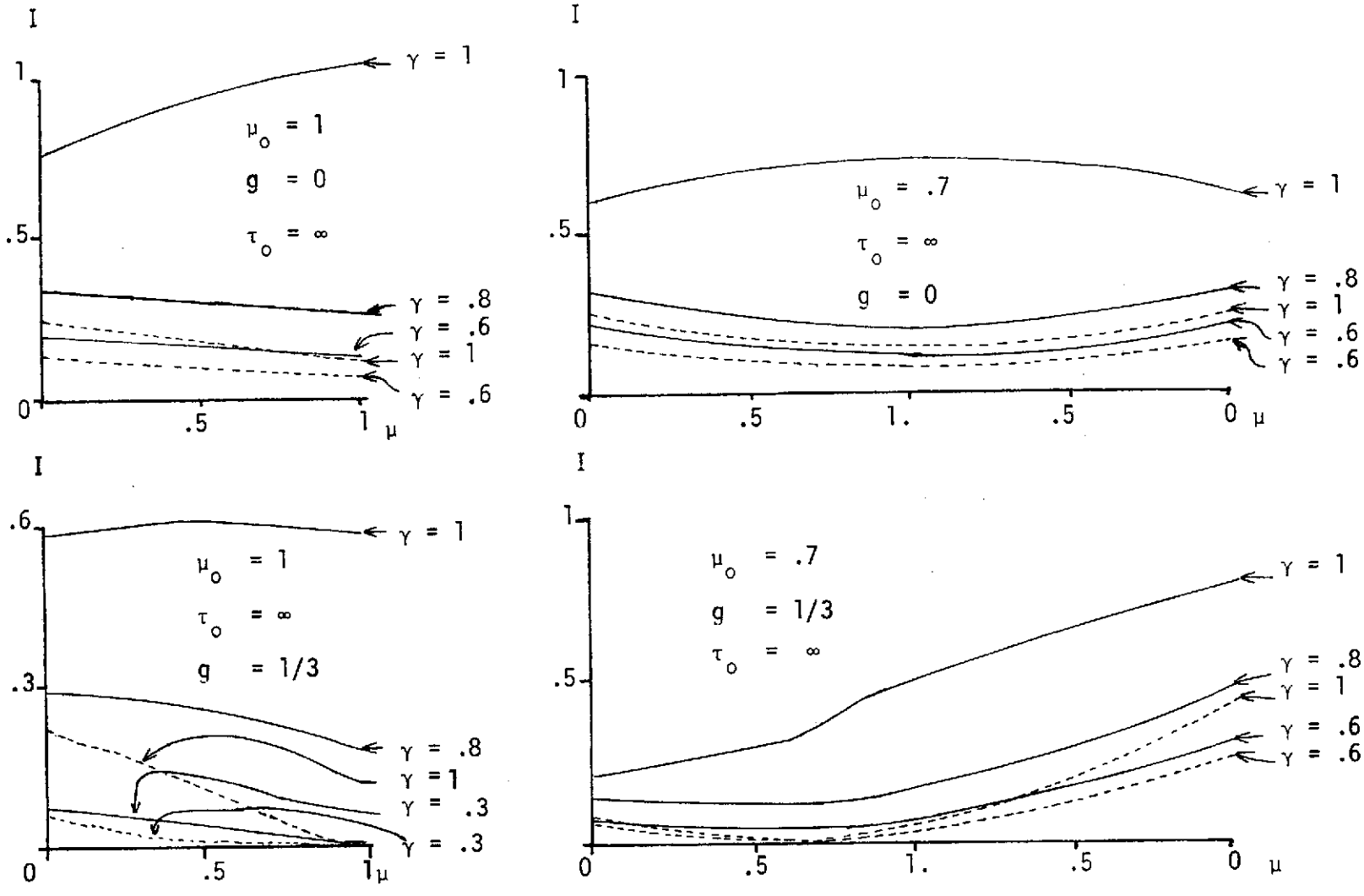

Figure XI Plots of Single and Multiple Scattering Results

The assumed values of parameters are given on each plot. In those cases for which μ ranges from zero to zero, $\phi - \phi_o = 0$ values of scattered intensity are on the left. Exact solutions are solid curves; single scattered solutions are broken lines. Units are incident intensity.

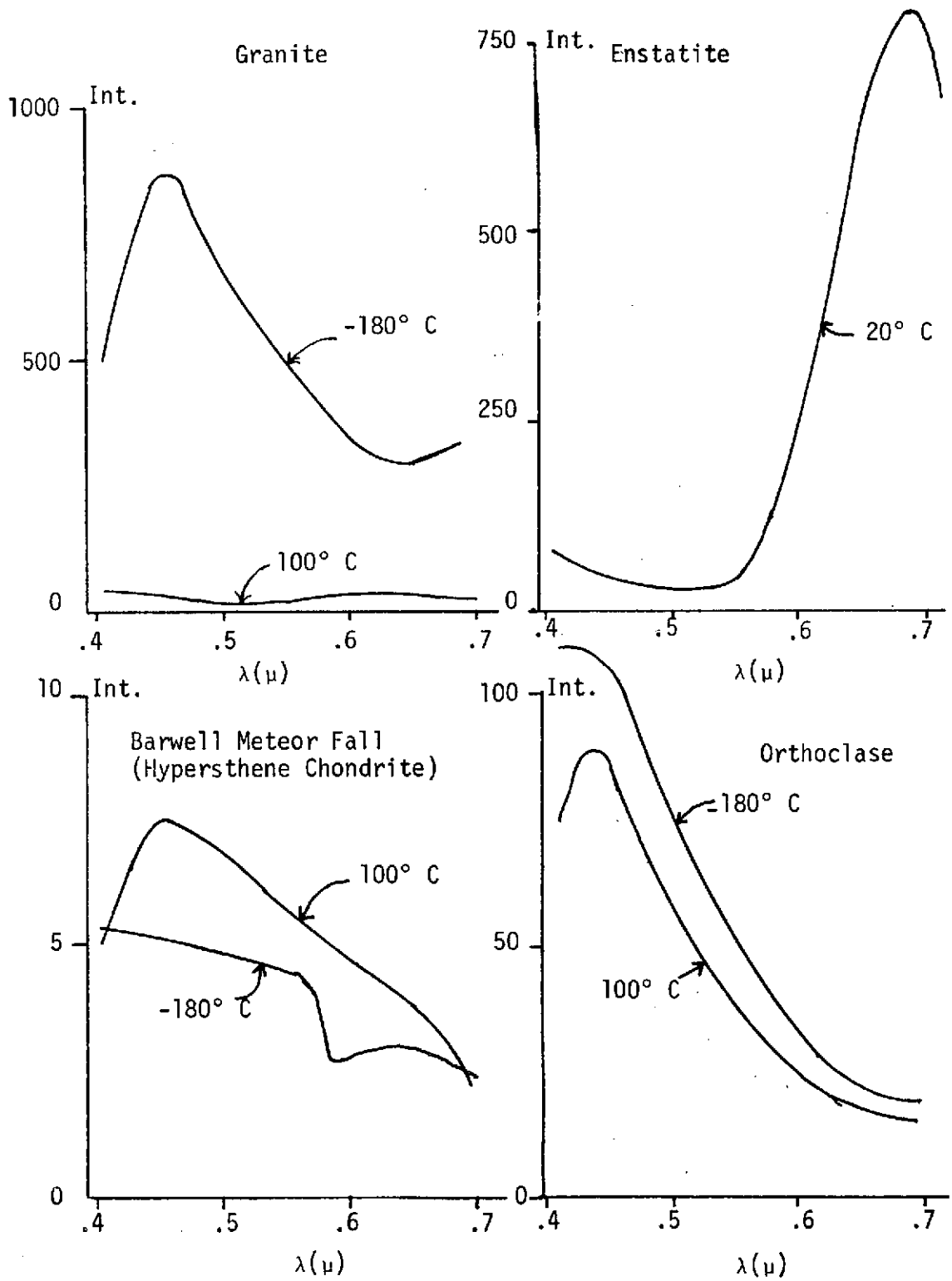

Figure XII Fluorescent Spectra of Some Minerals Excited by Proton Bombardment.

One unit is 2 x 10^6 photons/second. Note the increased fluorescence of granite at low temperature.

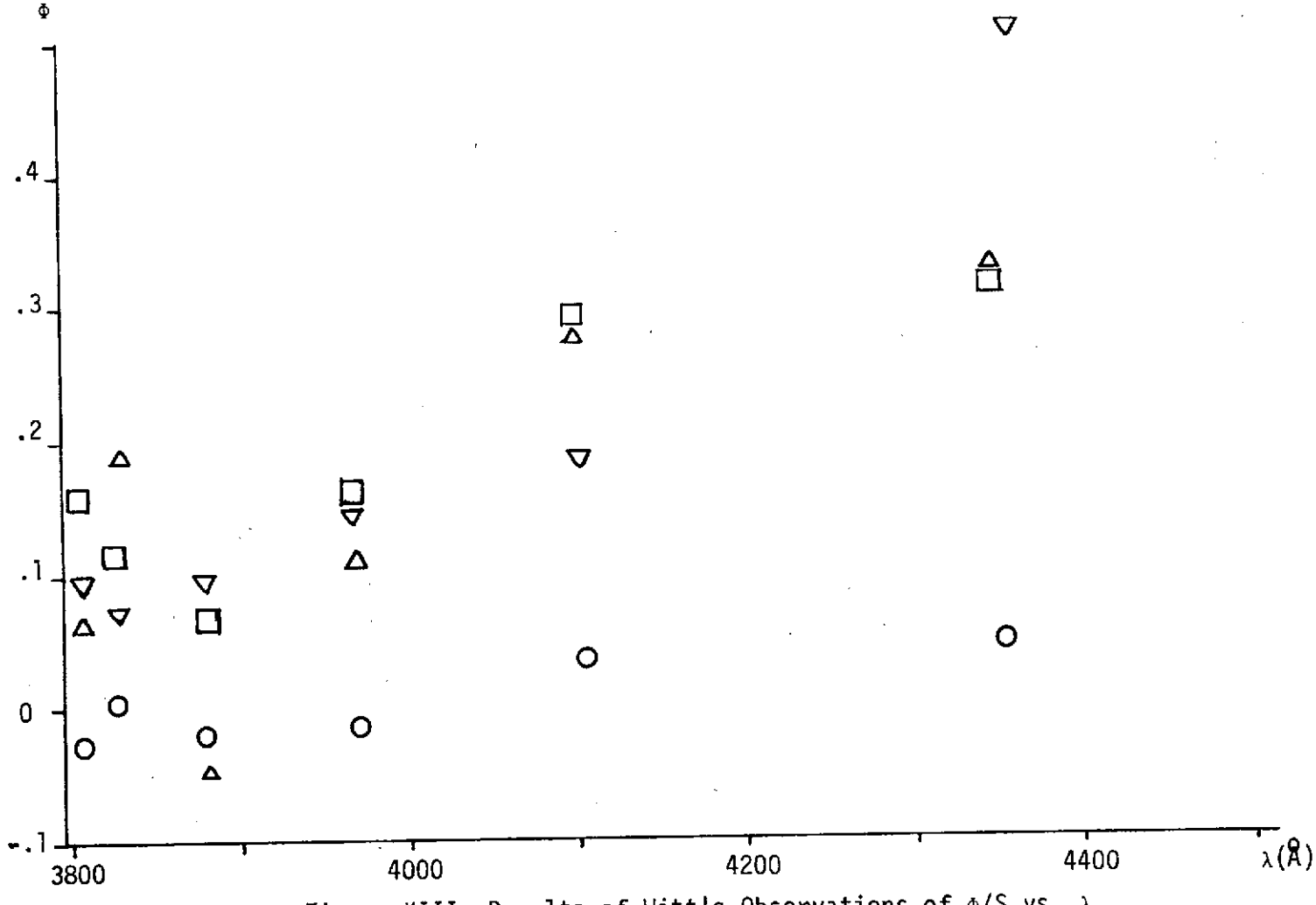

Figure XIII Results of Witt's Observations of Φ/S vs. λ

□ NGC 1435 △ NGC 2068 ▽ ξ^2 Ceti ○ 15 Sext

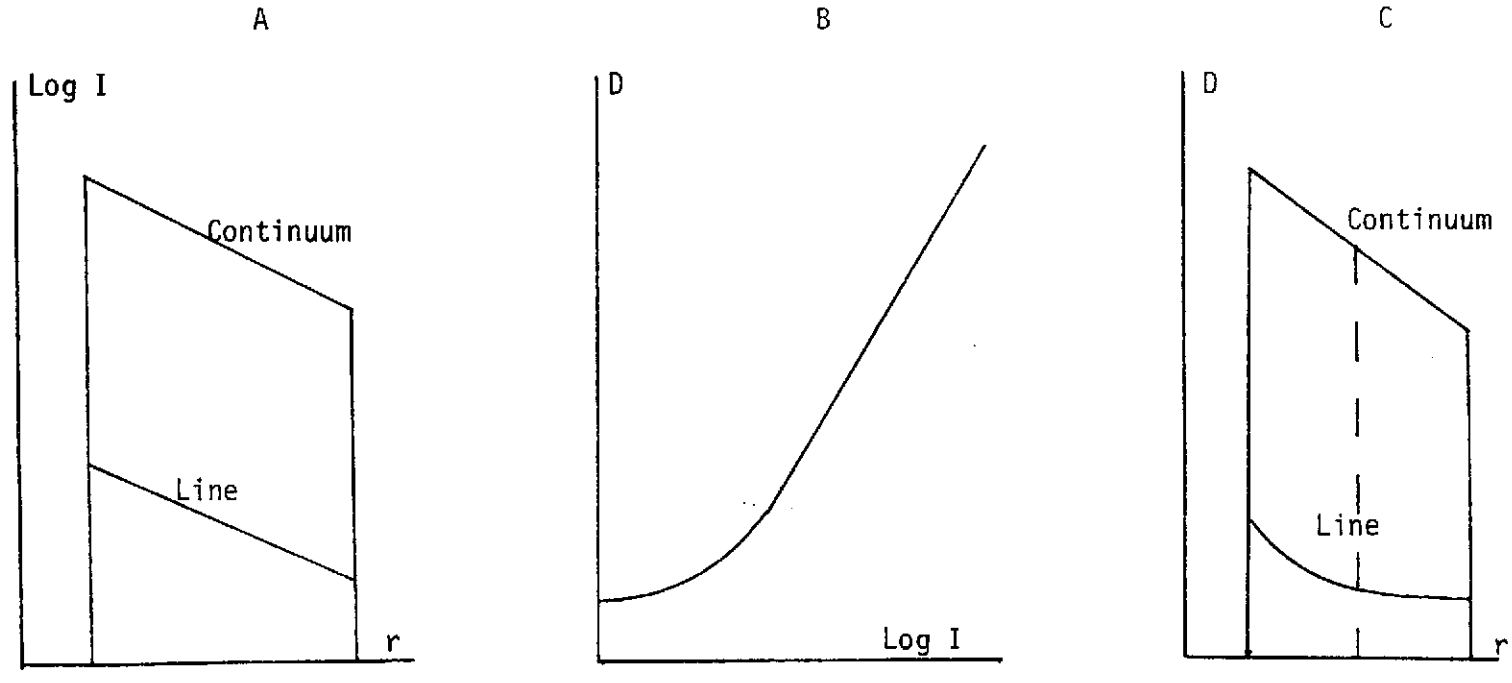

Figure XIV A. Intensity of Line and Continuum (reflected) vs. Distance from Star, r.

B. Photographic Characteristic Curve.

C. Photographic Plate Density vs. Distance From Star

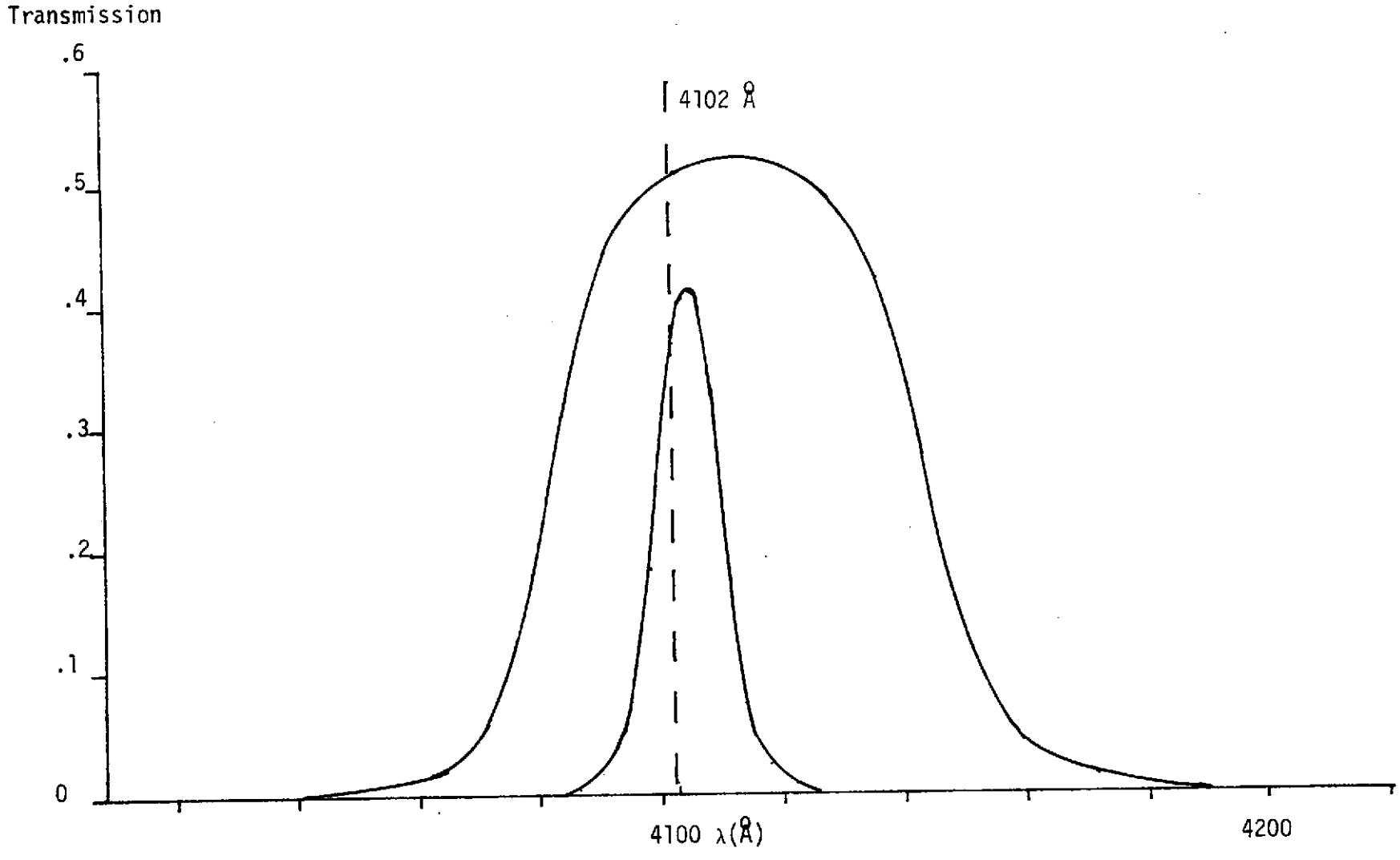

Figure XV Transmission as a Function of Wavelength for the H_δ Filter Pair

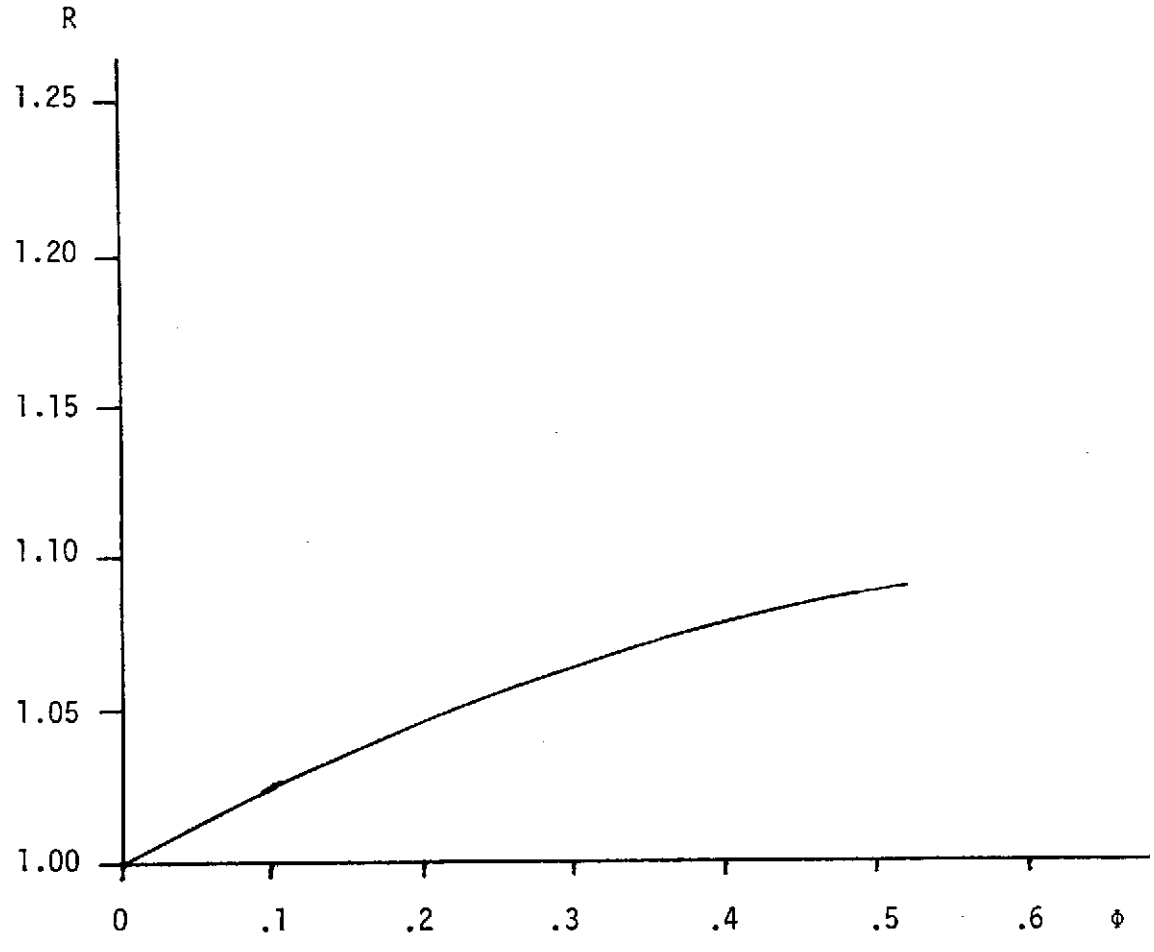

Figure XVI R as a Function of Φ for the H_δ Filter Pair

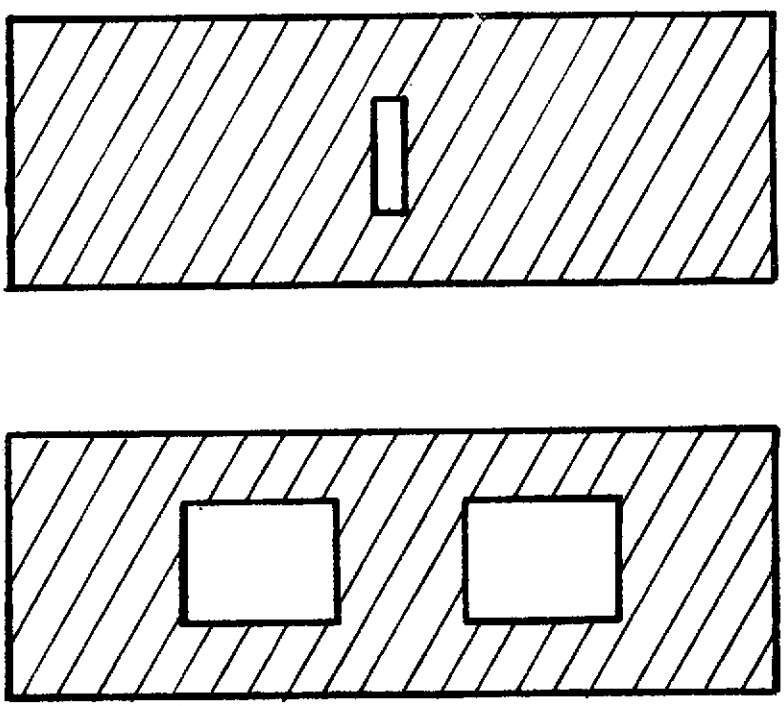

Figure XVII The "Three Slot" Exit Slots

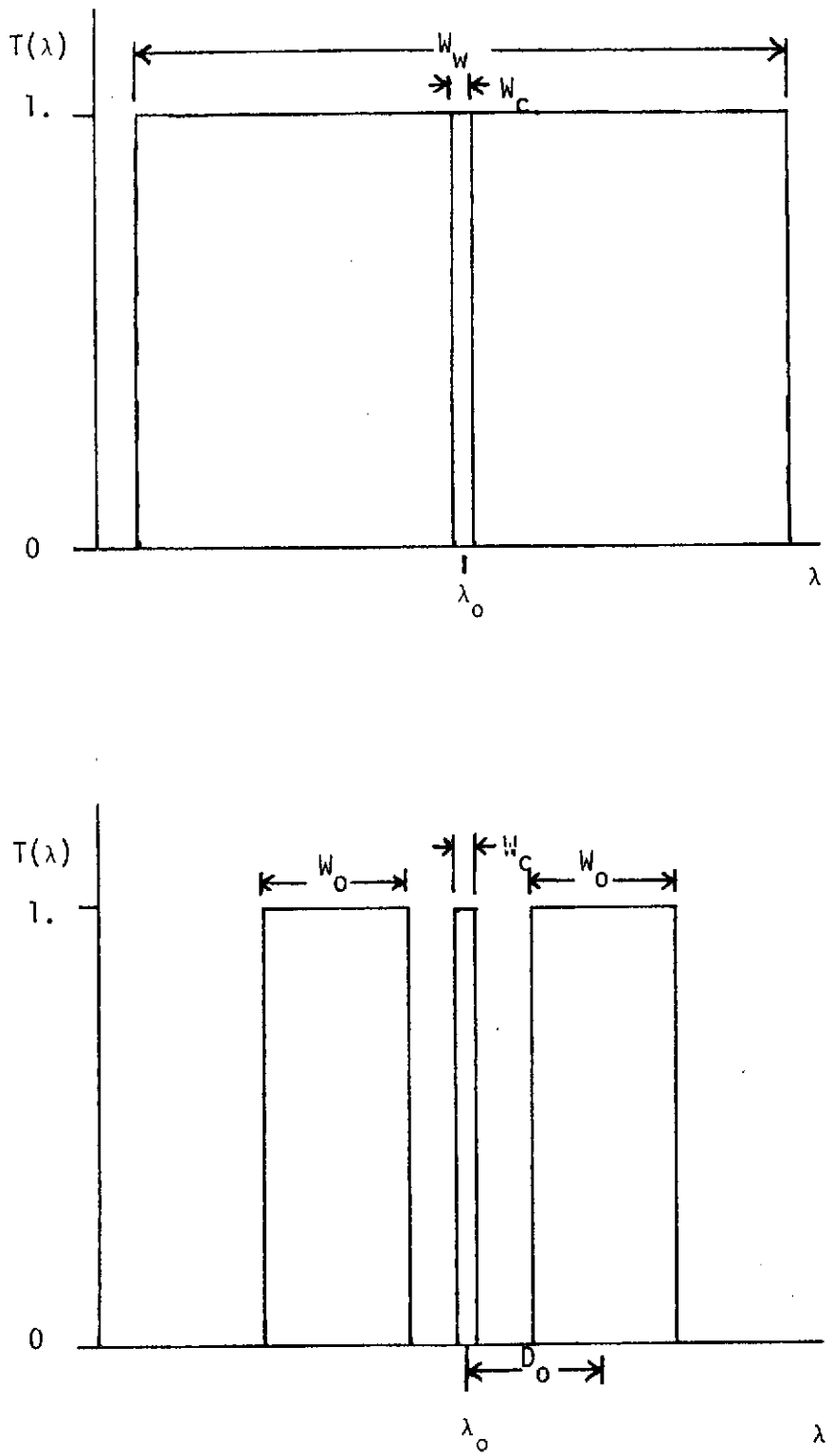

Figure XVIII The Two (Above) and Three (Below) Slot Transmission Curves

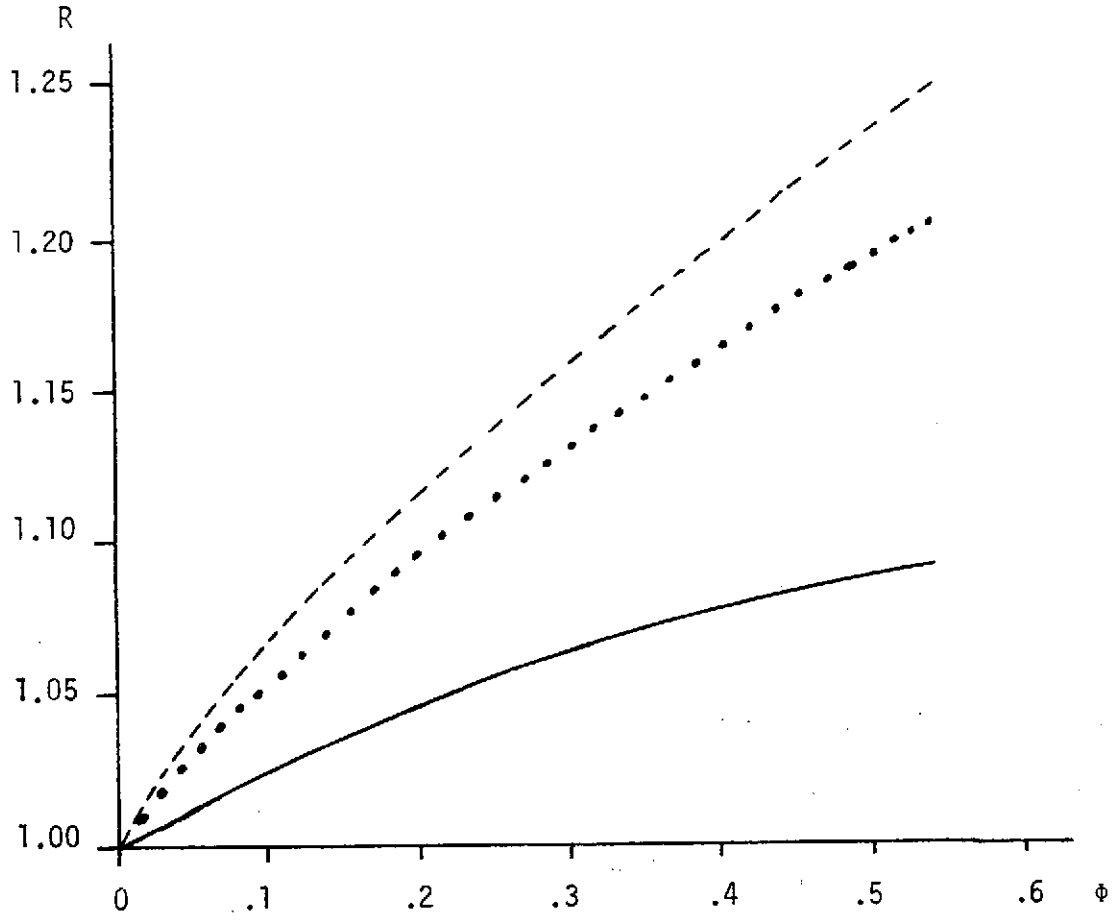

Figure XIX Variations of R with Φ.

The solid curve is the actual filter system used. The two slot (dotted line) and the three slot system (broken line) are also shown.

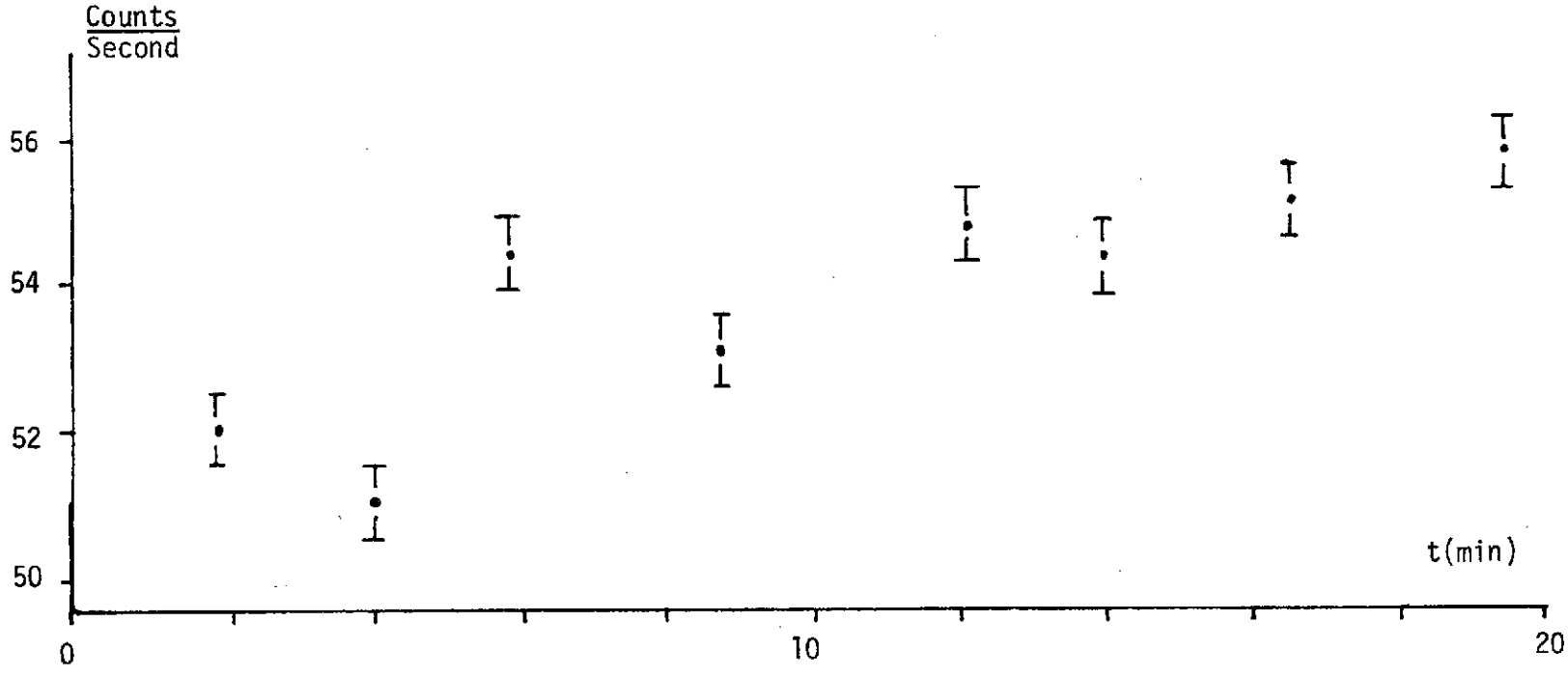

Figure XX Sky Brightness as a Function of Time for November 11, 1971

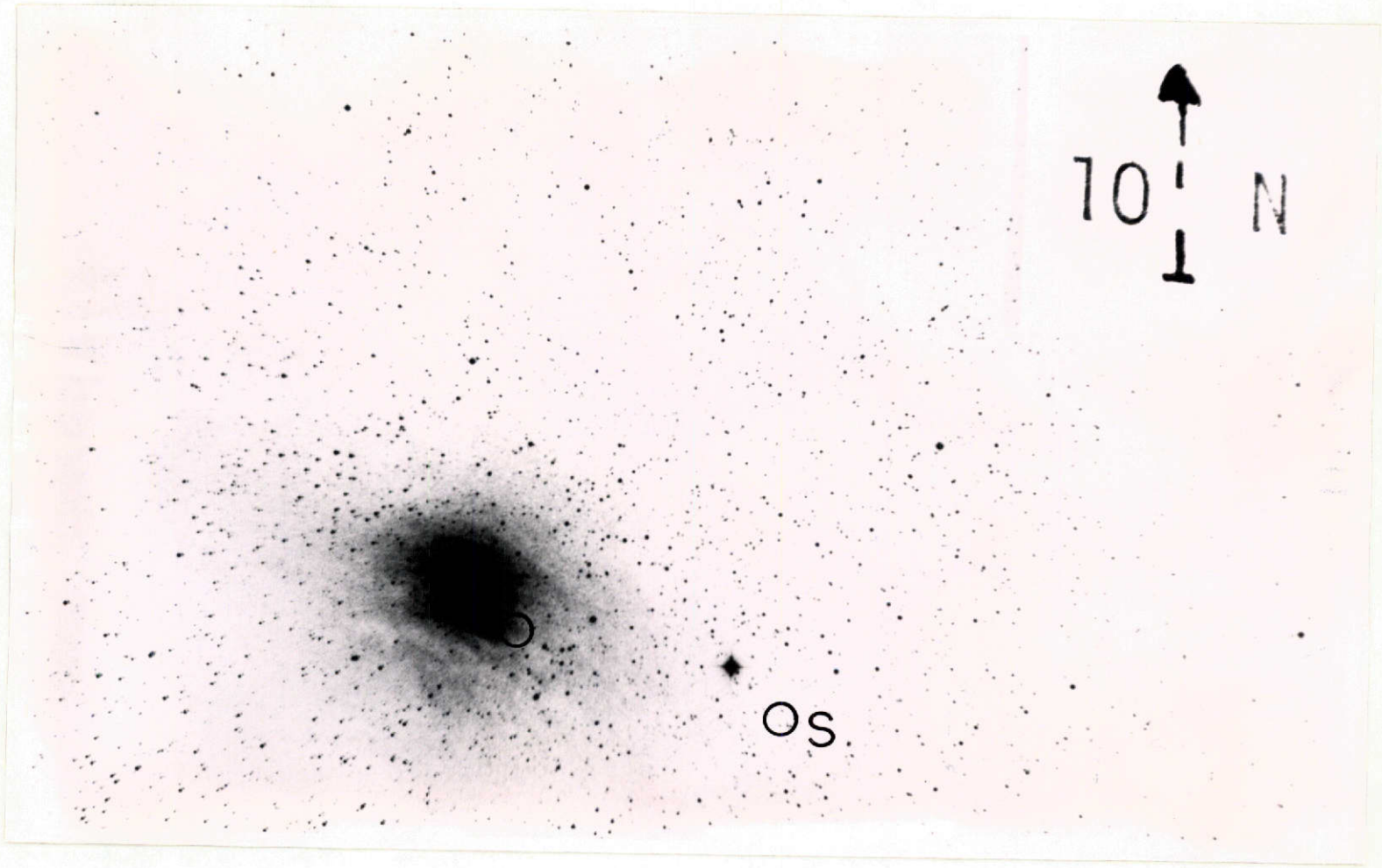

Figure XXI IC 1287 From Palomar Sky Survey (Red) Print.
The size of the inside edge of the circles is the diaphragm size used. The red print is shown here to indicate the relative position of the star and observation points.

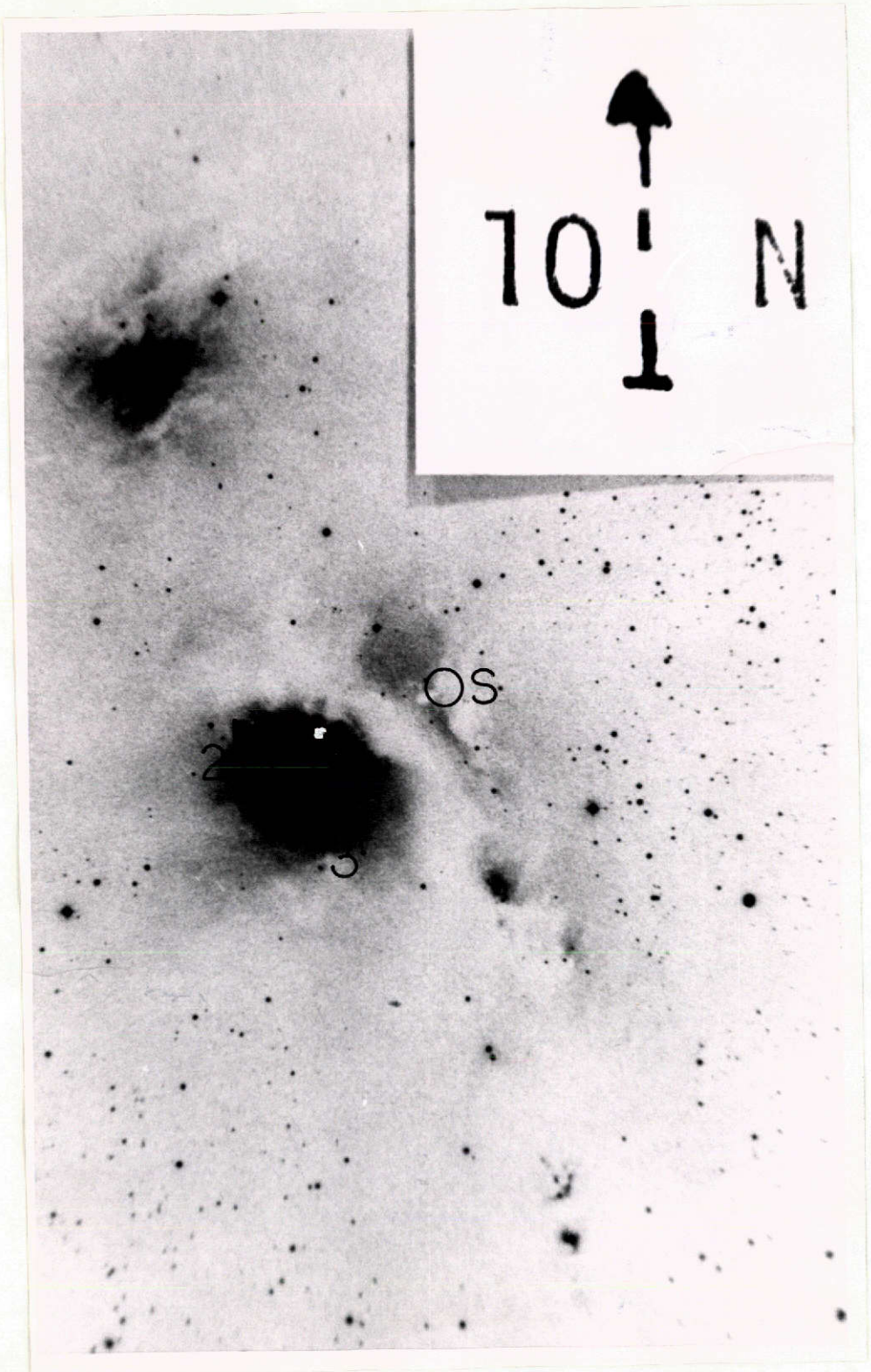

Figure XXII NGC 2068 From Palomar Sky Survey (Blue) Print.
The inside edge of the circles indicates the area of the diaphragm.
The position of the illuminating star is marked with a white dot.

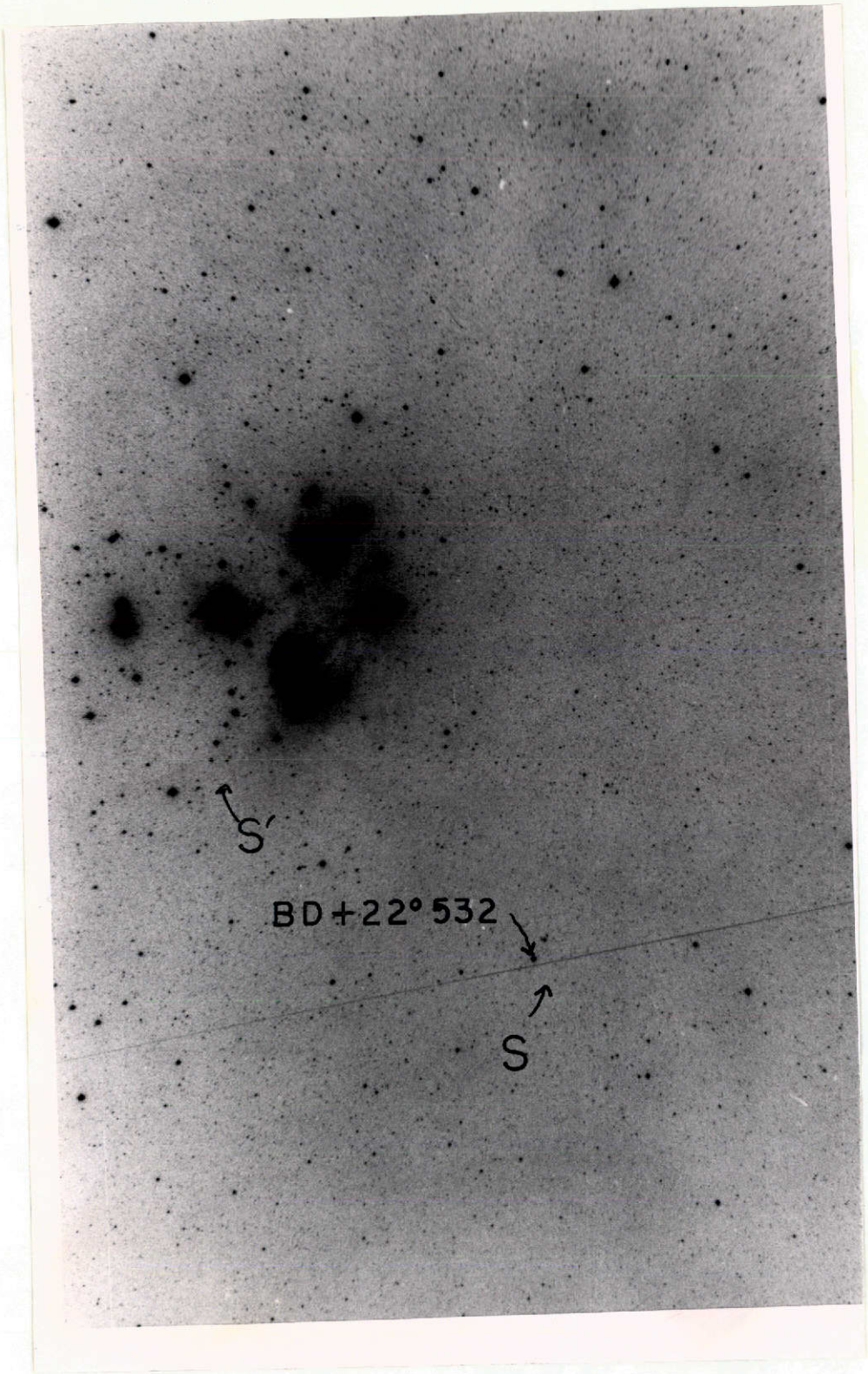

Figure XXIII The Region Surrounding NGC 1435 From Palomar Sky Survey (Blue) Print. The two sky observation points S and S' are indicated.

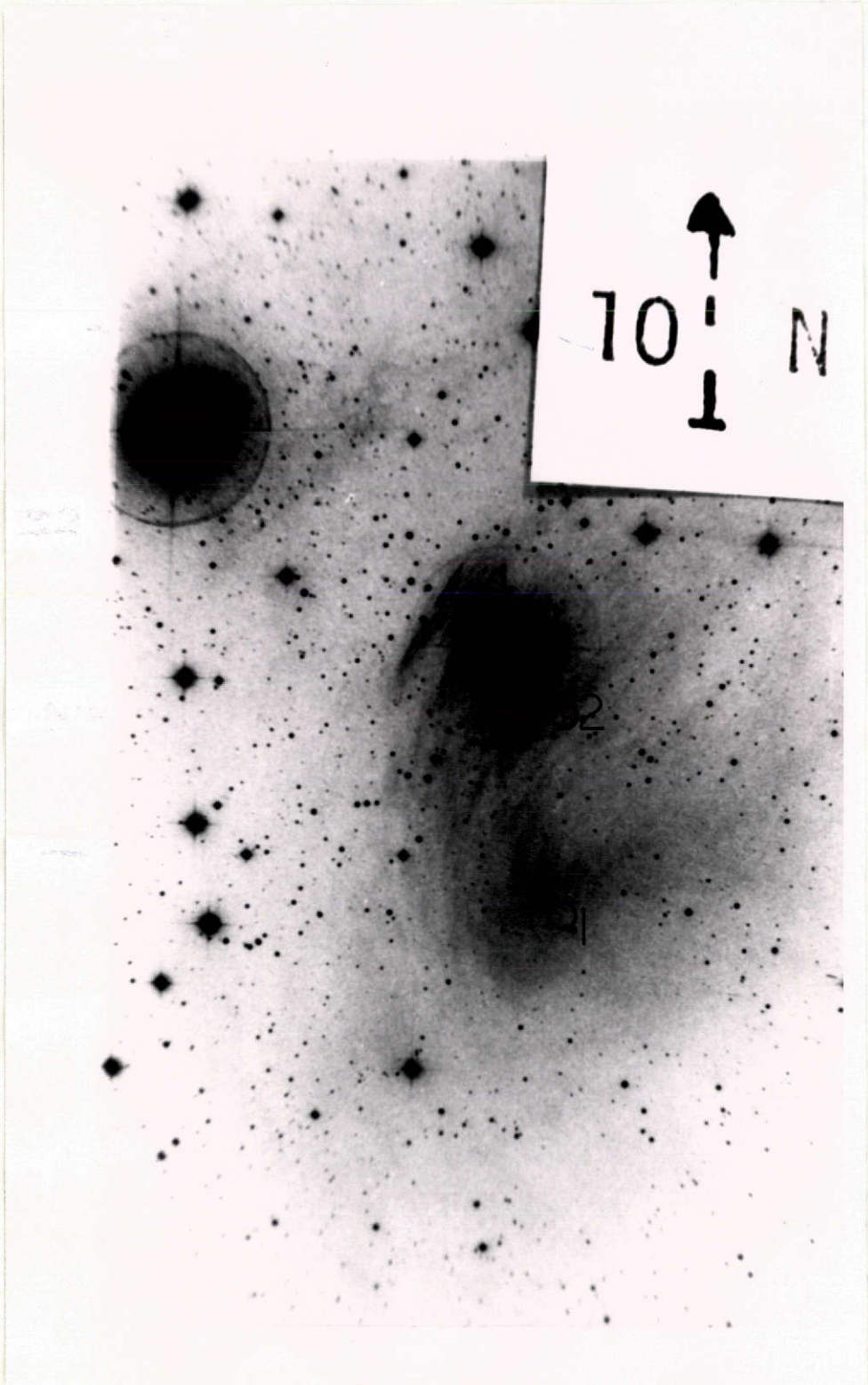

Figure XXIV NGC 1435 From Palomar Sky Survey (Blue) Print.
The inside edge of the circles denotes the diaphragm size.

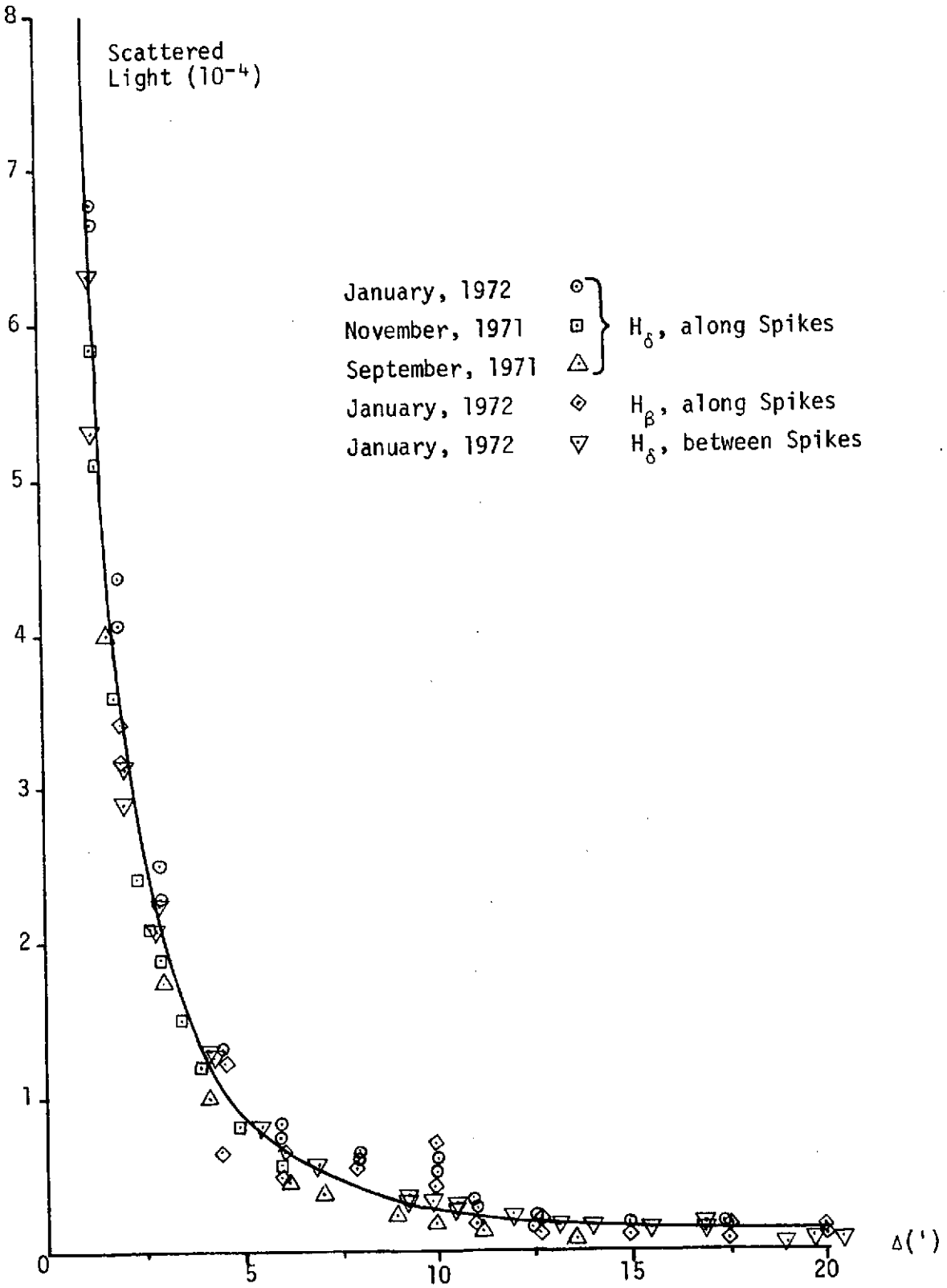

Figure XXV Scattered Light As a Function of Offset Angle
Scattered light is normalized to the stellar count rate.

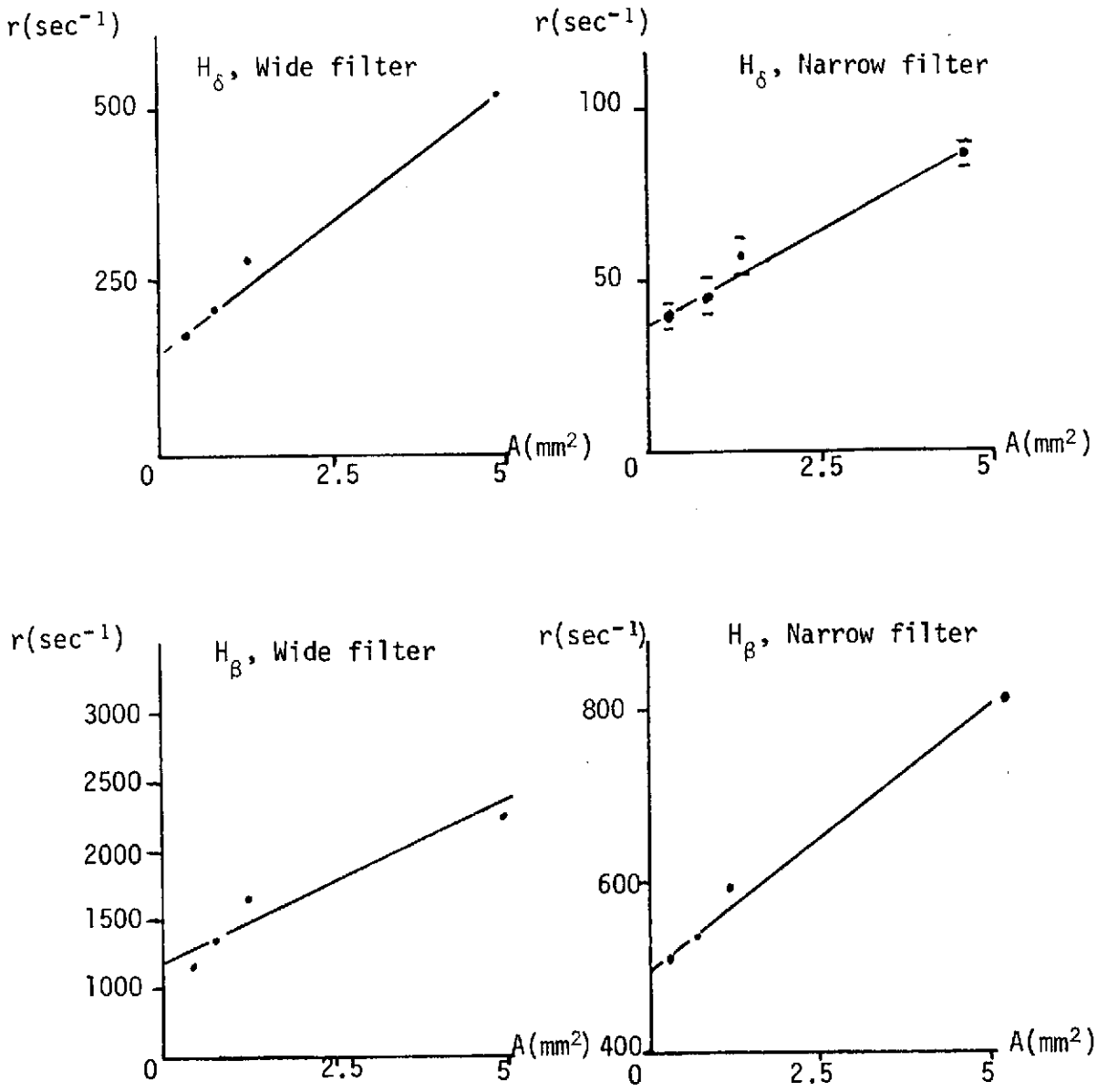

Figure XXVI Plot of Count Rate As a Function of Area for Several Runs.

The extrapolation to zero area gives the stellar count rate, free of nebula background. Error bars are statistical uncertainties. All observations are on NGC 2068.

Table I General Stellar Field Correction Coefficients

τ_o	γ=1	γ=.9	γ=.8	γ=.7	γ=.6	γ=.5	γ=.4	γ=.3
.6	.12	.10	.08	.06	.05	.04	.03	.02
1.0	.17	.13	.10	.08	.06	.04	.03	.02
2.0	.23	.16	.11	.08	.06	.04	.03	.02
∞,g=0	.50	.30	.14	.11	.08	.06	.04	.03
∞,g=.33	.31	.20	.11	.08	.05	.03	.02	.01

Table II The Multiple Scattering Correction Coefficients

	τ_o	γ=1	γ=.9	γ=.8	γ=.7	γ=.6	γ=.5	γ=.4	γ=.3
Front	.6	.20	.16	.12	.09	.07	.05	.04	.03
	1.0	.27	.21	.15	.10	.07	.05	.03	.02
	2.0	.41	.29	.17	.11	.06	.04	.02	.01
	∞,g=0	.82	.57	.17	.11	.06	.04	.02	.01
	∞,g=.33	.46	.32	.17	.11	.06	.04	.02	.01
Rear	.6	.19	.14	.10	.08	.06	.04	.02	.02
	1.0	.21	.15	.10	.07	.05	.03	.02	.01
	2.0	.21	.12	.04	.03	.03	.02	.01	.00

Table III Summary of Results of Model Calculations

Observer	I_o $\frac{S_{10}}{\square^\circ}$	m_{lim} $\frac{m}{\square''}$	H_o	τ_o	$\gamma(g=0)$	$\gamma(g=1/3)$
Hubble (1922)	66	23.25	11.1	.6	>1	>1
				1.0	.9	1.0
				2.0	.63	.75
				3.0	.38	.51
Dorschner & Gürtler (1966) Blue	66	23.6	12.0	.6	>1	>1
				1.0	>1	>1
				2.0	.82	.84
				3.0	.55	.67
Dorschner & Gürtler (1966) Red	116	22.4	10.8	.6	>1	>1
				1.0	>1	>1
				2.0	.83	.88
				3.0	.57	.69
Dorschner & Gürtler (1966) Blue + 10% fluorescence	66	23.6	12.0	.6	>1	>1
				1.0	>1	>1
				2.0	.79	.84
				3.0	.51	.65
Dorschner & Gürtler (1966) Blue + 30 % fluorescence	66	23.6	12.0	.6	>1	>1
				1.0	.98	>1
				2.0	.72	.80
				3.0	.45	.60

Table IV Results of the Observations

Object	λ(Å)	Pos.	NS(')	EW(')	R	σ	t(sec)
IC 1287	4102		2.7 S	2.2 W	1.026	.066	2750
NGC 1435	4861	2	1.9 S	1.9 W	.997	.020	1750
"	"	1	10.5 S	1.9 W	.971	.013	1750
"	4102	2	1.9 S	1.9 W	1.017	.023	5150
"	"	1	10.5 S	1.9 W	.984	.029	7050
NGC 2068	4861	1	0.0	1.0 E	.974	.014	1750
"	"	2	1.0 S	1.0 E	.981	.012	1250
"	"	3	2.5 S	0.0	.941	.005	500
"	4102	1	0.0	1.0 E	.937	.015	4500
"	"	2	1.0 S	1.0 E	.944	.020	3500
"	"	3	2.5 S	0.0	.946	.015	1750
15 Sext	4102		1.3 S	1.3 W	1.015	.010	2450

TABLE V

Listed below are some of the symbols used in this thesis. In addition to the symbol, the page on which it is defined and a brief definition are included. Symbols used on only one page are omitted.

Symbol	Page	Meaning
a	12	distance in arc minutes from star to edge of nebula
B	68	surface brightness in count rate/diaphragm area
c	21	conversion factor from radians to arc seconds
$C(\gamma,\tau_o,g)$	33	correction function for multiple scattering
D	31	correction function for illumination by the general star field
D	19	geometric thickness of nebula
D_o	59	displacement of center of outer exit slot from line center
$d\omega$	5	differential solid angle in square seconds of arc
$d\omega'$	21	differential solid angle in steradians
F	25	incident flux
g	5	asymmetry parameter
$G(\alpha)$	21	geometric factor
$H(\gamma,\mu)$	25	tabulated function
I_{GSF}	31	surface brightness due to illumination by the general star field
I_{lim}	30	limiting surface brightness which can be detected under standard conditions
I_n	20	flux leaving the nebular surface
I_o	27	integrated surface brightness of the Milky Way, averaged over a hemisphere

TABLE V (cont.)

Symbol	Page	Meaning
I_s	31	component of nebular surface brightness due to the illuminating star
L	12	luminosity of illuminating stars
m_{lim}	41	plate limit for an extended object, in magnitudes per square second
m_n	22	surface brightness of the nebula in magnitudes per square second
m_*	12	apparent magnitude of the illuminating star
P	12	an arbitrary point within the nebula
P (cos θ)	5	phase function
q	35	difference between observed and theoretical Hubble relation
r	12	distance from star to observer
R	12	distance from observer to nebula
R	57	see equation 41
R_*	73	narrow to wide count rate ratio for the star
t	71	integration time in seconds
W_c	59	width of central exit slot
W_o	59	width of outer exit slot
W_w	59	width of wide exit slot
x	23	phase function parameter
X	25	tabulated function
Y	25	tabulated function
α	12	angle from star to Earth as seen from nebula
α_i	18	angle of incidence
α_s	18	angle of reflection
γ	5	albedo

TABLE V (cont.)

Symbol	Page	Meaning
Δ	31	fraction of general star field light reflected by nebula
θ	5	scattering angle
λ	68	wavelength
μ	20	cos α_s
μ_o	18	cos α_i
ρ	68	count rate
τ	85	optical distance from P to nebular surface in observer's direction
τ_o	85	total optical thickness of nebula
τ_1	85	optical distance from P to star
ϕ	26	azimuthal angle
Φ	50	fluorescence parameter